INVITED PAPER

An Overview of Ultra-Wide-Band Systems With MIMO

Multiple input and output antennas used in ultrawide band systems can provide increased data rates, or they can make increased range available through beamforming.

By Thomas Kaiser, *Senior Member IEEE*, Feng Zheng, *Senior Member IEEE*, and Emil Dimitrov

ABSTRACT | Ultra-wide-band (UWB) technology combined with multiple transmit and receive antennas (MIMO) is a viable way to achieve data rates of more than 1 Gb/s for wireless communications. UWB is typically applied to short-range and therefore mainly indoor communications in environments characterized usually by dense multipath propagation. For this type of environment, MIMO systems allow for a substantial increase of spectral efficiency by exploiting the inherent array gain and spatial multiplexing gain of the systems. In this paper, we provide a brief overview for UWB-MIMO wireless technology. The overview covers channel capacity, space–time coding (STC), and beamforming. It is shown that the spectral efficiency is increased *logarithmically* and *linearly,* respectively, for single transmit and multiple receive antennas (SIMO) and MIMO systems. For multiple transmit and single receive antenna (MISO) systems, a threshold for the data transmission rate exists such that the spatial multiplexing gain can be obtained if the data rate is lower than this threshold, but it is not beneficial to deploy multiple transmit antennas if the required data rate is higher than the threshold. Two STC schemes for UWB-MIMO are briefly discussed, and their performance comparison is presented. A discussion about antenna selection is also presented, and the performance comparison between antenna selection and equal gain combiner is provided showing the diversity gain for some scenarios. For the beamforming, it is shown that the optimal beamformer is obtained if all the weighting filters in each antenna branch are identical. About the optimal beamformer, it is found that the amplitude of the side lobe is independent of the ray incidence angle, and the amplitude of the main lobe is increased by a fold of the element number in the array. Three kinds of beam patterns are defined, and the beamwidth of the main lobe is given. Experimental results based on an offline testbed are provided to verify some analytical results presented in this paper. Since UWB-MIMO is still in its research infancy, the aim of this paper is to present some first results on spatial multiplexing, STC, and beamforming to illustrate the potential of UWB-MIMO.

KEYWORDS | Beamforming; channel capacity; MIMO; space–time coding; ultra-wide-band communications

I. INTRODUCTION

High-data-rate wireless communications, nearing 1-Gb/s transmission rates, are of interest in emerging wireless local-area networks (WLANs) and home audio/visual network applications such as high-speed high-definition television (HDTV) audio/visual streams [58]. Currently, WLANs offer peak rates up to 54 Mb/s, and a target of 600 Mb/s is promised to be realized in the near future, e.g., in IEEE 802.11n WLANs [26]. The IEEE 802.15.3c wireless personal area networks will allow very high data rate over 2-Gb/s applications such as high-speed Internet access, streaming content download (video on demand, HDTV, home theater, etc.), real-time streaming, and wireless data bus for cable replacement. Optional data rates in excess of 3 Gb/s will be provided. However, to

Manuscript received November 27, 2007; revised September 7, 2008. First published February 27, 2009; current version published March 18, 2009.
The authors are with the Institute of Communications Technology, Faculty of Electrical Engineering, Leibniz University of Hannover, 30167 Hannover, Germany (e-mail: thomas.kaiser@ikt.uni-hannover.de; feng.zheng@ikt.uni-hannover.de; emil.dimitrov@ikt.uni-hannover.de).

Digital Object Identifier: 10.1109/JPROC.2008.2008784

achieve more than 50 Mb/s data rates, some technologies such as multiple transmit and multiple receive antennas (MIMO) and orthogonal frequency-division multiplexing (OFDM) should be adopted, as recommended in IEEE 802.11n. To reach the target of 1 Gb/s, more advanced techniques should be used. Ultra-wide-band (UWB) technology combined with MIMO might provide a solution.

As is well known, a UWB system [6], [48], [70], [79] can make use of huge frequency bands from 3.1 to 10.6 GHz in the United States [21] and Asia [17], and at least 6.0 to 8.5 GHz[1] in Europe [32], respectively. This provides a great potential for increasing the data transmission rate according to the Shannon theorem. However, due to the regulation imposed by the Federal Communications Commission (FCC) in the United States [21] and the European Commission document in Europe [32], the permitted power spectral density of the UWB signal is rather limited. This again limits data transmission rates. Incorporating the MIMO technique into UWB provides a viable solution for the bottleneck problem of power limit. For example, if a space–time coding (STC) is used, the power for a specific transmitted symbol will be strengthened, while the overall transmitted power is still the same as that of a single transmit antenna system, thus satisfying the FCC regulation (see Section III). If a beamforming technique is employed, the power of the signal in a specific direction is increased and may violate the power spectral mask in this direction, while the power in all other directions is still the same as the case without using the beamformer (see Section IV about the side-lobe discussion of UWB beamformers).

One may argue about why UWB should be combined with the MIMO technology since UWB itself offers rich diversity due to its abundant multipaths. A simple answer to this question is that it is due to the general greed of those pursuing higher data rates and higher quality of communications, but this is not the whole picture for the problem. According to Edholm's law of data rate [15], it can be predicted that indoor data rates of several gigabits/second will become reality in a couple of years. Therefore, although UWB offers enormous bandwidth and hence rich diversity in the time domain, even more bandwidth will be required in the near future. Hence, if it can be shown that the channel capacity of UWB systems is proportional to the number of transmit/receive antennas (this is indeed the case; see Section II), data rates can be significantly increased further by combining UWB and MIMO. This reason is the same as the one that triggered the research era on MIMO about two decades ago [80]. Even if lower data rates are in focus, the tradeoff between bandwidth and the number of antennas could facilitate the antenna and amplifier design, which is still a challenge for UWB systems. For example, the bandwidth requirement could be almost reduced by half if two antennas, instead of one antenna, on both transmitter and receiver sides are deployed.[2] For the design of UWB antennas, readers are referred to [5], [62], and [63].

In this paper, we will investigate the possibility and benefits of combining UWB and MIMO. We will highlight three aspects of this promising research field: channel capacity, space–time coding, and beamforming. The channel capacity describes a limit of the benefits in some sense for a UWB system employing multiple antennas, while the space-time coding provides a realization tool towards reaching the limit. UWB beamforming is of great importance for indoor localization, which has become a hot topic in UWB applications.

Compared to volumes of literature in the narrow-band MIMO research, there are only a few studies on the UWB-MIMO. The results on the channel capacity of UWB-MIMO systems can be found in [44], [59], [83], [84], and [86]. For the space–time coding, the first result was reported in [82] for impulse UWB systems, where the case of two transmit antennas and one receive antenna was considered. In [73], a spatial multiplexing coherent scheme for UWB-MIMO (2×2) system was experimentally investigated. In [75], the performance of a space–time trellis code for a 2×2 UWB-MIMO system was evaluated. For general MIMO impulse UWB systems, the STC schemes were derived in [1]–[3] and [64]. For OFDM-based UWB systems, [65] presented a STC method, essentially similar to the STC for wide-band OFDM. The report [76] introduced an approach to increasing the spatial diversity via antenna selection across data frames. It was found in [45] that polarization diversity is sometimes more effective than temporal (multipath) diversity in overcoming fading and reducing the required transmit energy. In [39], the spatial/temporal diversity was experimentally shown. In [13], a space–time selective Rake receiver was proposed considering the presence of narrow-band interference and multiple-access interference. In [27], a time interleave multiple transmit antenna UWB system was proposed where N_f monocycle pulses per information symbol are transmitted discontinuously through the time interleaver to get more temporal diversity. Spatial diversity and temporal diversity were compared therein. In [40], a zero-forcing scheme was proposed to remove the interference among the multiple data streams in UWB-MIMO systems. A space–time trellis coding scheme was proposed in [55]. In [68], [69], and

[1]In Europe, actually the frequency band from 1.6 to 10.6 GHz can be used, but a more strict spectrum mask is specified than in the United States. For details, see [32].

[2]Consider the case where we want to achieve a fixed data rate, say, R_0, by using a SISO UWB system (denoted as S_1) and a 2×2 MIMO UWB system (denoted as S_2), respectively. Except bandwidth, all other system parameters and configurations, e.g., modulations and coding-decoding techniques, are the same for S_1 and S_2. Suppose the bandwidth required by system S_1 to achieve R_0 is B_1. Since the channel capacity of S_2 is doubled compared to that of S_1 if they have the same bandwidth, system S_2 will require only a bandwidth of $B_1/2$ to achieve the same data rate R_0.

[77], the multiple-access performance of UWB-MIMO systems was investigated. About UWB beamforming, systematic studies for the problem were presented in [34], [35], and [60], with several fundamental differences being found. In [37], a digital UWB beamforming was proposed. The effect of multipaths on the beamformer output was illustrated in [53], which is simulated by using the ray-tracing technique. In [24], [25], and [38], the UWB beamformer was used to find the location of the source. In [43], an adaptive beamformer for multiband UWB wireless systems was proposed, where it is shown that the signal bandwidth has little impact on the beamwidth or direction, and hence the beam-focusing capability will not be sensitive to the signal bandwidth. In [67], the measured transient response of a uniform linear UWB array shows a peaked output without side lobes. In [31], an interesting algorithm for calculating the weighting coefficients for wide-band beamformers was developed.

One of the key problems in the UWB-MIMO study is the channel measurements and characterization, on which several reports have been published; see [39], [42], and [45].

Overall, the research on UWB-MIMO is still in its infant stage. Further studies, especially on its implementation, are necessary to bring this technology into the market.

The rest of this paper is organized as follows. In Section II, the UWB channel capacity is discussed. In Section III, two space–time encoding–decoding approaches are illustrated, and the performance of the antenna selection is investigated. In Section IV, the UWB beamforming problem is dealt with. In Section V, the experimental results based on the testbed in our lab are presented. Concluding remarks are given in Section VI.

Notation: The notation in this paper is fairly standard. $\mathbf{I}$ is an identity matrix whose dimension is indicated by its subscript if necessary; $P_A(x)$ and $p_A(x)$ represent, respectively, the cumulative distribution function and probability density function (pdf) of a random variable A; and $\mathcal{E}$ (or $\mathcal{E}_A$ if necessary) stands for the expectation of a random quantity with respect to the random variable A. The notation $\mathbf{R}_{\mathbf{x}}$ (or R_x) stands for the correlation matrix (or coefficient) if the corresponding subscript $\mathbf{x}$ (or variable x) is a random variable, and R_w stands for the autocorrelation function if the corresponding subscript w is a deterministic waveform. For a matrix or vector, the superscripts ^{T} and † denote the transpose and Hermitian transpose, respectively, of the matrix or vector. The notation † also applies to a scalar. Throughout this paper, the function log is naturally based.

II. UWB CHANNEL CAPACITY

In this section, we investigate the channel capacity of UWB-MIMO systems. It gives a picture for how much potential the systems combining together the UWB and MIMO technology can provide. As channel capacity depends on the statistical properties of the channel, we need first to examine the statistic model for the multipath fading of a UWB-MIMO wireless system, which is the starting point of this section and also serves as some basis for the sections to be followed.

A. Channel Model

Let us start from the channel model of a single-transmit and single-receive antenna (SISO) system. Generally, a UWB communication channel can be expressed in terms of multipath delays and the corresponding fading gains [12]

$$h(t) = \sum_{l=1}^{L} \alpha_l \delta(t - \tau_l) \tag{1}$$

where $h(t)$ is the impulse response of the physical channel, δ the Dirac delta function, L the number of multipath components, τ_l the excess delay of the lth delay bin (we assume that $\tau_1 = 0$, i.e., the first delay bin is considered as the starting point of the reference), and α_l the amplitude fading in the lth delay bin. Several models for UWB channels have been proposed recently in [12], [16], [18], [28], and [47]. In [12], the Nakagami distribution is shown to fit the amplitude fading; In [16] and [18], it is claimed that the amplitude fading admits a lognormal distribution [16] and a Weibull distribution [18], respectively. In [28] and [47], the lognormal distribution is proposed to approximate the amplitude fading, and it is also found that both lognormal and Nakagami distributions can fit the measurement data equally well. These different models are due to the different measurement environments. For the convenience of analysis, we use the Nakagami distribution to model the amplitude fading in this section. All the results in [12], [16], [18], [28], and [47] show that the excess delay can be modeled by a Poisson process.

Let us denote α_l as

$$\alpha_l = \nu_l \zeta_l$$

where $\nu_l := \mathtt{sign}(\alpha_l)$ is the sign of α_l, and $\zeta_l := |\alpha_l|$ is the magnitude of α_l. The statistics of the fading of ζ_l is modeled by the Nakagami distribution, whose general form is described by the following pdf:

$$p_{\zeta_l}(x) = \begin{cases} 2\left(\frac{\kappa}{2\Omega_l}\right)^{\frac{\kappa}{2}} \frac{1}{\Gamma\left(\frac{\kappa}{2}\right)} x^{\kappa-1} e^{-\frac{\kappa x^2}{2\Omega_l}} & \text{when } x \geq 0, \\ 0 & \text{when } x < 0, \end{cases} \quad \kappa \geq 1 \tag{2}$$

where Γ denotes the Gamma function, $\Omega_l = \mathcal{E}(\alpha_l^2)$, and $\kappa = 2[\mathcal{E}(\alpha_l^2)]^2/\mathrm{Var}[\alpha_l^2]$. Throughout this paper, it is

assumed that the number κ is a constant and the same for all delay bins.

The power of the amplitude fading is exponentially decreasing with the excess delay. Therefore, it is reasonable to assume that Ω_l varies with l according to the following model:

$$\Omega_l = r\Omega_{l-1} \tag{3}$$

where $r < 1$ is a constant. According to the data reported in [12], [14], r takes a value between 0.91 and 0.98. Of course, the value of r is determined by the scenario of communications. In this section we will assume that $r = 0.95$.

The variable ν_l takes the signs $+1$ and -1 with equal probability to account for signal inversion due to reflections.

Generally, the excess delay τ_l is also a random variable, but in many studies (see, e.g., [81]), it is treated as a deterministic variable $\tau_l = (l-1)\tau$ for the reasons of both analytical convenience and sampling processing at the receiver, where τ is the sampling period. This model is especially suitable to dense scattering environments [48]. In this paper, we will also adopt this convention.

Let $X(t)$ and $Y(t)$ denote the transmitted UWB signal and the received signal after the matching filter and sampling, respectively. Then the relationship between $X(t)$ and $Y(t)$ can be described by

$$Y(t) = \sum_{l=1}^{L} \alpha_l X(t-(l-1)\tau) + N(t) \tag{4}$$

where $N(t)$ denotes the receiver noise and τ can be set to be $1/B$, with B being the bandwidth of the transmitted signal X. In channel capacity calculation, we can assume that the transmitted signal will occupy the whole bandwidth of the channel frequency band.

In the MIMO case, the input–output relation (channel model) can be generally described, similar to (4), by the following equation:

$$\mathbf{Y}(t) = \sum_{l=1}^{L} \mathbf{A}_l \mathbf{X}(t-(l-1)\tau) + \mathbf{N}(t) \tag{5}$$

where $\mathbf{X}(t)$ and $\mathbf{Y}(t)$ are N_T- and N_R- dimensional vectors of transmit and receive signals, respectively, with N_T and N_R being the numbers of the transmit and receive antennas; $\mathbf{A}_l$, $l = 1, \ldots, L$, the amplitude fading matrices; and $\mathbf{N}(t)$ is the receive noise vector. For a random process $\mathbf{X}(t)$ (vector-valued), define its power spectral density (PSD) matrix as $\mathbf{S}_{\mathbf{X}}(f) = \int_{-\infty}^{+\infty} \mathcal{E}[\mathbf{X}(t+\tilde{\tau})\mathbf{X}^T(t)]e^{-j2\pi f\tilde{\tau}}d\tilde{\tau}$. It is implied in the model (5) that the numbers of multipaths across all the MIMO channels are the same L. This is physically unrealistic. In practice, we can choose L as the number of time-bins of the longest channel and set the amplitude of the extraneous taps for the shorter channels to zero. For the channel model (5), we further make the following simplifying assumptions, as usual in discussing the channel capacity problem.

Assumption 1: The amplitude fading matrices $\mathbf{A}_l$, $l = 1, \ldots, L$, are assumed to be mutually independent, and all the entries of $\mathbf{A}_l$, $l = 1, \ldots, L$, are also assumed to be mutually independent. Suppose $\mathbf{A}_l = [\alpha_{l,mn}]_{N_R \times N_T}$ with $l = 1, \ldots, L$, $l = 1, \ldots, L$, $m = 1, \ldots, N_R$, $n = 1, \ldots, N_T$. Then $\zeta_{l,mn} = |\alpha_{l,mn}|$ is of the distribution (2) with Ω_l being governed by the model (3) and $\nu_{l,mn} = \mathtt{sign}(\alpha_{l,mn})$ takes values ± 1 with equal probability.

Assumption 2: The noise $\mathbf{N}$ is zero-mean Gaussian with PSD matrix being $N_0\mathbf{I}_{N_R}$.

Assumption 3: The power of the transmitted signal is bounded by $\bar{S}$, i.e.,

$$\mathcal{E}\left(\mathbf{X}^T(t)\mathbf{X}(t)\right) = \int_{-\frac{B}{2}}^{\frac{B}{2}} \mathtt{tr}(\mathbf{S}_{\mathbf{X}}(f))df \le \bar{S} \tag{6}$$

where $\mathtt{tr}$ denotes the trace of a square matrix.

We presume that the receiver possesses a complete knowledge of the instantaneous channel parameters, i.e., the realizations of $\mathbf{A}_l$ and their statistics. However, we assume that the transmitter is not aware of the information about channel parameters except in the cases pointed out elsewhere.

B. Channel Capacity

The Shannon capacity of a communication channel is the maximum transmission rate supportable by the channel. For an additive white Gaussian noise channel, whose input–output relationship is characterized by $y(t) = x(t) + n(t)$, the channel capacity is given by Shannon's well-known formula [19]

$$C = B_x \log\left(1 + \frac{\mathcal{E}(x^2)}{\mathcal{E}(n^2)}\right) \tag{7}$$

where x, y, and n are the transmitted signal, received signal, and receiver noise, respectively, and B_x is the

channel bandwidth. Equation (7) provides a fundamental relationship among the system capacity, channel bandwidth, and the average signal-to-noise power ratio (SNR) characterized by $\mathcal{E}(x^2)/\mathcal{E}(n^2)$. Shannon's coding theorem proves that there exists a code for x that achieves data rates arbitrarily close to the capacity C with arbitrarily small probability of bit errors for a sufficiently long coding block.

For the channel of wireless narrow-band communications, the input–output relationship is characterized by

$$y(t) = ax(t) + n(t) \tag{8}$$

where a is a random variable characterizing the fading caused by the communications environment. Since the SNR at the receiver $a^2\mathcal{E}(x^2)/\mathcal{E}(n^2)$ is also a random variable, two notions of capacity, namely, ergodic capacity and outage capacity, are introduced [7], depending on the property of the fading a.

First, if the fading changes so quickly that the transmitted codeword experiences many (or an infinite number of, in the extreme case) independently fading blocks, the ergodic capacity defined as

$$C_e = B_x\mathcal{E}_a\left[\log\left(1+\frac{a^2\mathcal{E}(x^2)}{\mathcal{E}(n^2)}\right)\right] \tag{9}$$

gives a characterization for the data rates supportable by the channel. The ergodic capacity represents the average data rate supportable by the channel.

Secondly, if the fading changes so slowly that a transmitted codeword spans only a single fading block (in other words, the fading is almost a constant in one codeword), the outage capacity defined as

$$P_{\text{out}}(R) = P_{C|_a}(R) \tag{10}$$

gives a characterization for the data rates supportable by the channel, where R is the data transmission rate and $C|_a$ is the channel capacity for a given realization or sample of the fading. The so-defined $P_{\text{out}}(R)$ means that if some codewords are transmitted across the channel with the rate R, the codewords cannot be correctly decoded with a probability of $P_{\text{out}}(R)$, i.e., the channel can only support the rate R with a probability of $1-P_{\text{out}}(R)$.

For an MIMO channel described by

$$\mathbf{y}(t) = \mathbf{x}(t) + \mathbf{n}(t) \tag{11}$$

where $\mathbf{y}$, $\mathbf{x}$, and $\mathbf{n}$ are N_x-dimensional vectors and $\mathbf{n}$ is a white Gaussian noise vector, the channel capacity is obtained by maximizing the mutual information given by [71]

$$\begin{aligned}\mathcal{I}(\mathbf{x};\mathbf{y}) &= 2B_{\mathbf{x}}[\mathcal{H}(\mathbf{y}) - \mathcal{H}(\mathbf{n})] \\ &= B_{\mathbf{x}}\log\det\left[\mathbf{I}+\mathbf{R}_{\mathbf{x}}\mathbf{R}_{\mathbf{n}}^{-1}\right]\end{aligned} \tag{12}$$

under constraints applied on the transmitted signal $\mathbf{x}$, where $\mathcal{H}$ denotes the differential entropy of a continuous variable and $B_{\mathbf{x}}$ is the bandwidth occupied by $\mathbf{x}$. Note that the unit of $\mathcal{I}$ is nats/s. A typical constraint on $\mathbf{x}$ is that the power carried by $\mathbf{x}$ is limited (see Assumption 3).

It is clear that (12) is a direct extension of (7) in the MIMO case. The matrix $\mathbf{R}_{\mathbf{x}}\mathbf{R}_{\mathbf{n}}^{-1}$ can be considered as a generalized SNR. Since multiple antennas are deployed in the MIMO case, we can allocate the overall power across the transmit antennas in different ways. For example, for a wireless MIMO system, the channels between different pairs of transmit–receive antennas may experience severely different fading. If the transmitter has this prior knowledge, more power can be allocated to the better channel while less power to the worse channel, so that the overall data transmission rate can be increased. Therefore, some optimization procedures are needed to maximize the mutual information given by (12).

The channel capacity for model (5) can be obtained by combining the results (9) and (12) for the models (8) and (11), respectively. Define $\mathcal{A} = (\mathbf{A}_1, \ldots, \mathbf{A}_L)$. For a given realization of $\mathcal{A}$, the conditional channel capacity of (5) is as follows [49], [83]:

$$C|_{\mathcal{A}} = \int_{-\frac{B}{2}}^{\frac{B}{2}} \log\det\left[\mathbf{I}_{N_R} + \frac{1}{N_0}\mathbf{H}(f)\mathbf{S}_{\mathbf{X}}(f)\mathbf{H}^{\dagger}(f)\right]df \tag{13}$$

where $\mathbf{H}(f) = \sum_{l=1}^{L}\mathbf{A}_l e^{-\mathrm{j}2\pi f(l-1)\tau}$. The PSD of the transmitted signal $\mathbf{X}$, $\mathbf{S}_{\mathbf{X}}(f)$, should be chosen to maximize the integral in (13) subject to the power constraint (6). In (13), $(1/N_0)\mathbf{H}(f)\mathbf{S}_{\mathbf{X}}(f)\mathbf{H}^{\dagger}(f)$ can be considered as the generalized SNR of the channel at the center frequency f. The channel capacity of the whole UWB channel can be viewed as the integral of small pieces of narrow-band channels.

In principle, the power spectrum $\mathbf{S}_{\mathbf{X}}(f)$ should be optimized across two dimensions—frequency domain and spatial domain—if the channel matrix $\mathbf{H}(f)$ or, equivalently, the matrices $\mathbf{A}(1), \ldots, \mathbf{A}(L)$, are known at the transmitter. Since the transmitter does not have any information about $\mathbf{H}(f)$, the best way for distributing the power in the transmitter is to equally allocate it among all

antennas and to uniformly distribute it over the frequency band $[-(B/2), +(B/2)]$. Thus we have

$$\mathbf{S}_{\mathbf{X}}(f) = \begin{cases} \frac{\bar{S}}{N_T B}\mathbf{I}_{N_T}, & \text{when } f \in \left[-\frac{B}{2}, \frac{B}{2}\right] \\ 0, & \text{otherwise.} \end{cases} \tag{14}$$

Therefore, substituting (14) into (13) gives the conditional channel capacity $C|_{\mathcal{A}}$ as follows:

$$\begin{aligned} C|_{\mathcal{A}} &= \int_{-\frac{B}{2}}^{\frac{B}{2}} \log\det\left[\mathbf{I}_{N_R} + \frac{1}{N_0}\frac{\bar{S}}{N_T B}\mathbf{H}(f)\mathbf{H}^{\dagger}(f)\right] df \\ &= \frac{B}{\pi}\int_0^{\pi} \log\det\left\{\mathbf{I}_{N_R} + \frac{\rho}{N_T}\left[\sum_{l=1}^{L}\mathbf{A}_l e^{-\mathrm{j}(l-1)u}\right]\right. \\ &\qquad \left.\times\left[\sum_{l=1}^{L}\mathbf{A}_l^T e^{\mathrm{j}(l-1)u}\right]\right\} du \end{aligned} \tag{15}$$

where ρ stands for the SNR:

$$\rho = \frac{\bar{S}}{BN_0}.$$

Since it is extremely difficult, if possible, to obtain the closed-form expression for the integral in (15), we use the Monte Carlo method to evaluate the distribution of $C|_{\mathcal{A}}$, denoted as $P_{C|_{\mathcal{A}}}(x)$. In the simulation, we will first find the distribution of $\bar{C}|_{\mathcal{A}} := C|_{\mathcal{A}}/B$, the spectral efficiency for a realization of $\mathcal{A}$. Notice that, thanks to (15), the integral in the simulation needs only to be taken over $[0, \pi]$ instead of over $[0, B/2]$. This fact would relieve our computational burden.

With $P_{\bar{C}|_{\mathcal{A}}}(x)$, the outage probability of the channel capacity can be obtained by

$$P_{\text{out}}(R) = P_{C|_{\mathcal{A}}}(R) = P_{\bar{C}|_{\mathcal{A}}}\left(\frac{R}{B}\right)$$

for a given data transmission rate R.

Remark 1: Note that the power spectrum allocation policy (14) is justified from the information theoretic perspective, but in practice this policy can be only approximated due to the power spectrum mask and the particular waveforms used.

Remark 2: There is a lot of research work on the capacity of narrow-band MIMO fading channels (see, e.g., [29] and [71] for analytical studies and [30] and [49] for measurement studies), but few reports are available on the study of the capacity of frequency-selective MIMO fading channels. References [8], [9], [44], and [49] are some examples of the research in this field.

C. Simulation Results

We study three cases: multiple transmit and single receive antenna (MISO), single transmit and multiple receive antennas (SIMO), and MIMO (we fix $N_T = N_R$ in this case for the convenience of exposition). In all the simulations, it is assumed that $\kappa = 4$, $\Omega_1 = 1$, and $r = 0.95$.

The results for the MISO case are depicted in Fig. 1. From this figure, it can be seen that for a given ρ, the outage probability decreases with the number of transmit antennas when R/B is lower than some value (denoted as R_1) but increases instead when R/B is higher than another value (denoted as R_2). Notice that the corresponding outage probability is so high when R/B is larger than R_2 that to transfer information at this rate is of little practical interest. Therefore, if the required transmission rate is indeed too high and the available power is limited, it is better to concentrate all the power on one antenna rather than to distribute the power among multiple antennas.

It is difficult to calculate R_2 exactly, which depends on the number of transmit antennas under comparison [86]. However, R_1 is given by [86]

$$R_1 = \log\left(1 + \frac{(1-r^L)\Omega_1}{1-r}\rho\right) := R_c.$$

We call R_c the critical transmission rate. Substituting the corresponding parameters for Fig. 1 into the above equation, we get $R_c = 4.68$ nats/s/Hz. From Fig. 1(b), it is observed that the gap between R_2 and R_c is not big.

A more clear picture about the critical transmission rate can be seen from the case of frequency-flat channels [85], where it is found that R_2 almost coincides with R_c. The same phenomenon is also found in narrow-band MISO systems in [71].

The results for the SIMO case are demonstrated in Fig. 2, which clearly shows that, for a given transmission rate, the outage probability decreases considerably with the number of receive antennas in the range of whole transmission rate, making a striking contrast to the case of MISO. In other words, we can say that the communication rate can be considerably increased for a given outage probability with the number of receive antennas. To see the quantitative relationship between N_R and the increased amount of the communication rate, we view Fig. 2 from another perspective. That is, first fix P_{out}; then for this P_{out}, find the communication rate R/B supportable by the

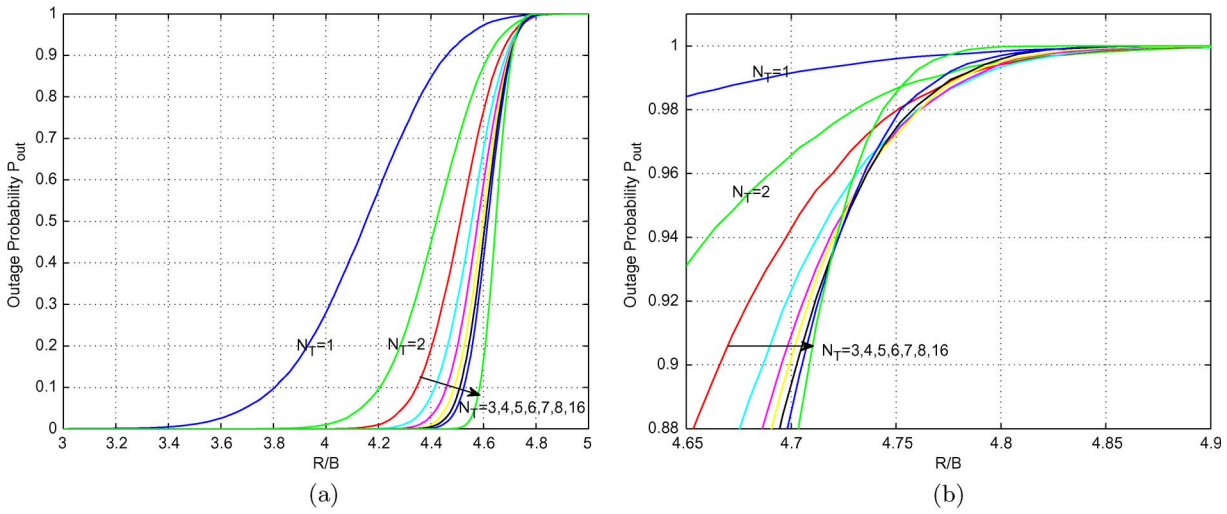

Fig. 1. *Outage probability P_{out} versus transmission rate R/B (in nats/s/Hz) for different N_T: effect of the number of transmit antennas on the channel capacity ($\rho = +10$ dB, $L = 15$, $N_R = 1$). (a) Panorama and (b) detail.*

channel corresponding to different N_R; and finally plot the curves showing the relationship between R/B and N_R for different P_{out}, which is depicted in Fig. 3. Notice that we have deliberately used $\log N_R$ as the abscissa of Fig. 3. This figure clearly reveals that R increases with $\log N_R$ almost linearly. This phenomenon can be observed more clearly in the scenario of high SNR. Basically, this is due to the linear increase in SNR with N_R under optimal combining of the received signals at the receiver. It is noticed that the variance of the channel capacity decreases with the number of receive antennas. This phenomenon is also observed in [41] and [49].

Fig. 4 shows the results for the MIMO case, from which we can again observe that, for a given transmission rate, the outage probability decreases with the number of transmit and receive antennas considerably in the range of whole transmission rate. To investigate the quantitative relationship between N_T (or N_R) and the increased amount of the communication rate, we plot Fig. 4 from another perspective, similar to the SIMO case. The result is shown in Fig. 5. From this figure, it can be seen that R increases with N_T (or N_R) linearly. This is a well-known property for narrow-band MIMO communication systems. This property also holds true for the UWB-MIMO systems because of the fact that the order of the integral and the summation inherited from log det in (15) is exchangeable. Suppose

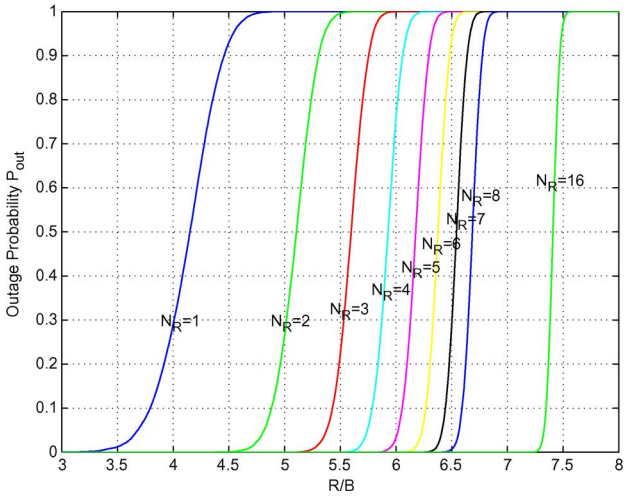

Fig. 2. *Outage probability P_{out} versus transmission rate R/B (in nats/s/Hz) for different N_R: effect of the number of receive antennas on the channel capacity ($\rho = +10$ dB, $L = 15$, $N_T = 1$).*

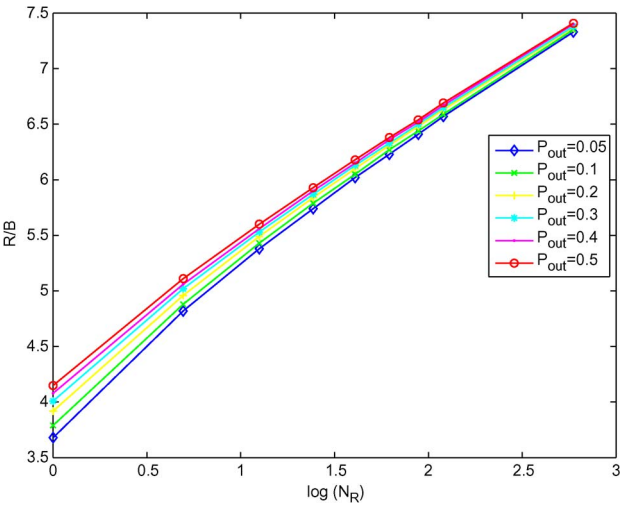

Fig. 3. *The transmission rate R/B (in nats/s/Hz) versus N_R for different outage probability P_{out} ($\rho = +10$ dB, $L = 15$, $N_T = 1$).*

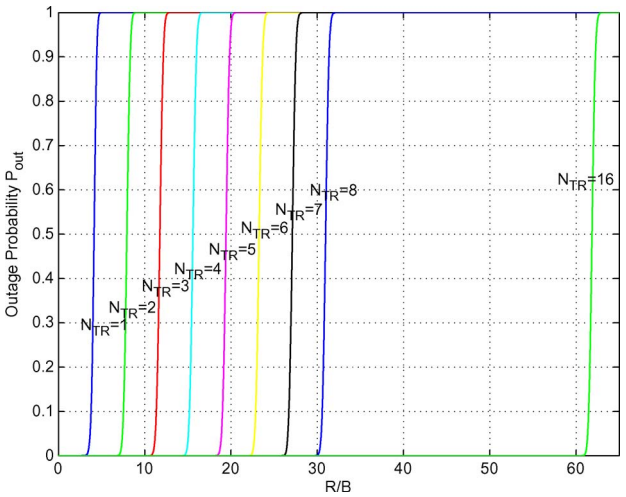

Fig. 4. *Outage probability P_{out} versus transmission rate R/B (in nats/s/Hz) for different N_T (or N_R): effect of the number of transmit and receive antennas on the channel capacity ($\rho = +10$ dB, $L = 15$, $N_T = N_R$, where $N_{TR} := N_T = N_R$).*

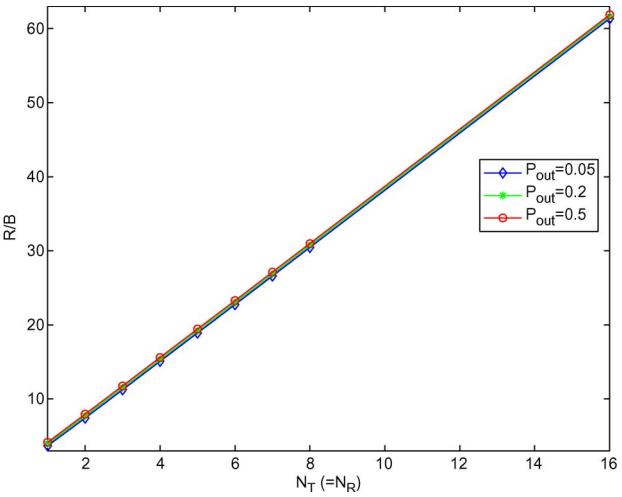

Fig. 5. *The transmission rate R/B (in nats/s/Hz) versus N_T (or N_R) for different outage probability P_{out} ($\rho = +10$dB, $L = 15$, $N_T = N_R$).*

that the matrix $\mathbf{H}(f)$ is of full rank.[3] By using the singular value decomposition of the matrix $\mathbf{H}(f)$, the matrix $\mathbf{H}(f)\mathbf{H}^{\dagger}(f)$ can be transformed into a diagonal form, with the diagonal entries being the singular values of $\mathbf{H}(f)$. Thus from (15), we can see that the capacity of UWB-MIMO systems is equal to that of the system with N_R parallel channels, and hence is N_R-fold of the capacity of UWB-SISO systems.

If the transmitter has the full channel state information, the transmit power can be optimally distributed across both frequency and spatial domains in terms of the instantaneous channel multipath fading, resulting in the water-filling algorithm in both domains. The detailed algorithm is presented in [86]. Fig. 6 illustrates the performance comparison between the optimal power spectrum allocation (OPSA) policy, as shown in [86], and the uniform power spectrum allocation (UPSA) policy, as shown in (14). We use $C_{\text{uni}}/C_{\text{opt}}$ as an index for the efficiency of UPSA relative to OPSA, where C_{uni} and C_{opt} denote the ergodic channel capacity under UPSA and OPSA policies, respectively. It is demonstrated that the efficiency of UPSA is lower than 0.61 when the SNR is lower than -20 dB. This indicates that the transmission rate can be increased roughly more than 1.6 times if OPSA, instead of UPSA, is adopted. But when $\rho \geq +10$ dB, $C_{\text{uni}}/C_{\text{opt}}$ almost approaches one. Therefore, the optimal power distribution algorithm such as the water-filling approach should be considered in the low SNR regime.

D. Channel Correlation

In the preceding development, we have assumed that 1) all the matrices $\mathbf{A}_l$, $l = 1, \ldots, L$, are independent of each other; and 2) all the entries of $\mathbf{A}_l$ for a given l are also independent of each other. Generally, the first assumption is reasonable since different matrices characterize the microwave propagations caused by different scatterers, but the second assumption is impractical since the matrix $\mathbf{A}_l$ describes the microwave propagations caused by the same group of scatterers. The correlation property among the entries of $\mathbf{A}_l$ characterizes the spatial correlation among the antennas. Similar to narrow-band MIMO channels, there are two approaches to model the spatial correlation among the antennas [57]. The first approach is to use a matrix of dimension $N_T N_R \times N_T N_R$ to describe the correlation between any two entries in $\mathbf{A}_l$. The second approach is to change the channel matrix as

$$\bar{\mathbf{A}}_l = \mathbf{R}_r^{\frac{1}{2}} \mathbf{A}_l \mathbf{R}_t^{\frac{1}{2}} \tag{16}$$

where $\mathbf{R}_r$ and $\mathbf{R}_t$ are the $N_R \times N_R$ receive covariance matrix and $N_T \times N_T$ transmit covariance matrix, respectively. This model is based on the assumption that the correlation among the receive antennas is independent of the correlation among the transmit antennas. For a uniform linear array of antennas, the matrix $\mathbf{R}_r$ (similar expression applies to the matrix $\mathbf{R}_t$) can be typically described by [57]

$$\mathbf{R}_r = \begin{bmatrix} 1 & \rho_c & \rho_c^2 & \cdots & \rho_c^{N_R-1} \\ \rho_c & 1 & \rho_c & \cdots & \rho_c^{N_R-2} \\ \rho_c^2 & \rho_c & 1 & \cdots & \rho_c^{N_R-3} \\ \vdots & \vdots & \vdots & \ddots & \vdots \\ \rho_c^{N_R-1} & \rho_c^{N_R-2} & \rho_c^{N_R-3} & \cdots & 1 \end{bmatrix} \tag{17}$$

[3]Since $\mathbf{H}(f)$ is a random matrix, the probability that $\mathbf{H}(f)$ is rank deficient will be zero.

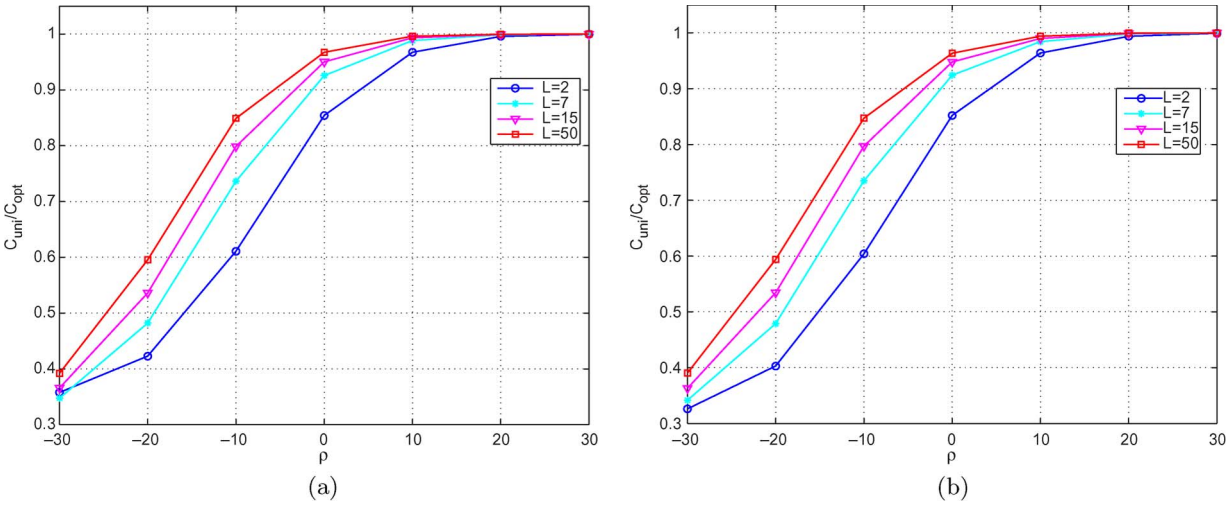

Fig. 6. *Efficiency of UPSA relative to OPSA. (a) $N_T = N_R = 4$ and (b) $N_T = N_R = 8$.*

where ρ_c is the correlation coefficient between two neighboring antennas. The correlation model defined by (17) captures the fact that the spatial correlation of the UWB channel decreases with the distance of the antennas. Note that the channel matrices for two different time delays are still assumed independent. The similar model in frequency domain is used in [4], where it is shown that the bit error rate (BER) performance of the MIMO systems based on the simulated channel using the above model gives a good approximation to the BER performance of the MIMO systems based on the measured channel if an appropriate ρ_c is chosen. The full characterization of the spatial correlation of the UWB channels is provided in [42], where it is found that in the range of 2.5 times of the coherence distance (about 4 cm), the antenna correlation follows a pattern of the first kind zeroth-order Bessel function of the distance, while almost a constant correlation coefficient (smaller than 0.4) is observed when the antenna distance is larger than the 2.5 times of the coherence distance. It is particularly interesting that, as shown in [22], [23], [42], [44], and [45], the antenna angular orientation and the signal polarization can be used to decrease the correlation of the spatial channels or to improve the system performance.

Another approach describing the spatial channel correlation property is from the deterministic point of view [73]. It is defined as the average value of all the cross-correlation functions of different spatial channels normalized by the autocorrelation functions of the corresponding spatial channels.

Generally, the channel capacity of MIMO systems will decrease when the mutual correlation of the spatial channels is strong because the diversity of the channels decreases due to the correlation. For narrow-band MIMO systems, this result can be easily seen from the singular value decomposition of the channel matrix [71]. In the extreme case, if the rank of the correlation matrices $\mathbf{R}_r$ and $\mathbf{R}_t$ reduces to one, the MIMO channel will collapse to a SISO channel. This phenomenon also exists in UWB-MIMO systems. A simulation result is shown in Fig. 7, where we fixed $N_T = N_R = 8$ and $L = 50$. For simplicity, the channel correlation model (16) is used and both $\mathbf{R}_r$ and $\mathbf{R}_t$ take the form of (17) and the same value of ρ_c. As shown in Fig. 7, the channel capacity decreases significantly with ρ_c if $\rho_c \geq 0.5$, while it almost keeps the same value as that of the uncorrelated channels if $\rho_c \leq 0.2$. Comparing [42, Fig. 2], we can claim that the channel capacity of UWB-MIMO systems will not suffer

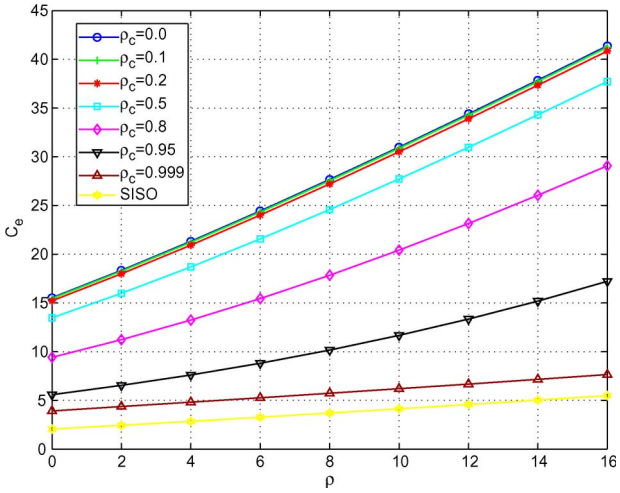

Fig. 7. *The effect of correlation coefficient of the spatial channels on the ergodic channel capacity of MIMO systems. Here $N_T = N_R = 8$ for MIMO and $L = 50$ for both MIMO and SISO.*

degradation if the antennas are separated from each other by more than 10 cm.

It is noteworthy that the channel correlation model (16) changes the form of the pdf of the fading of the single channel, i.e., the pdf of the entry of the matrix $\bar{\mathbf{A}}_l$ is no longer of the form of Nakagami or log-normal. This is different from the narrow-band MIMO channels where a linear transformation of the channel matrix only changes the parameters of the pdf of the fading matrix, but not the form. Notice also that model (16) is a simplified mathematical model for the channel correlation, whose validity, indirectly verified in [4], needs to be further examined through extensive UWB channel measurement studies.

III. PERFORMANCE OF SPACE–TIME CODING AND ANTENNA SELECTION

In the literature, a few papers have addressed the issue of exploiting transmit diversity for the impulse UWB system; see, e.g., [3], [76], [77], and [82]. In [77], the performance of pulse-amplitude modulated signals in the UWB-MIMO channel is evaluated. In [82], the authors innovated a space–time coding scheme for both binary pulse-amplitude modulation (PAM) or pulse-position modulation (PPM)-based UWB systems with two transmit antennas. The STC scheme in [82] is similar to Alamouti's STC scheme for narrow-band systems, which is easy for implementation. In [3], a general STC scheme for M-ary PAM and PPM UWB systems is proposed based on cyclic division algebra theory. However, it was shown that energy-efficient codes are possible only for *two* transmit antennas. In [76], a scheme of time-switched transmit diversity for impulse UWB systems was proposed and its performance investigated. It was shown that using multiple transmit antennas in the UWB channel can improve the system performance by reducing signal variations. However, using multiple transmit antennas does not provide diversity gain in the strict sense. This is in contrast to the result obtained in [82], where it was illustrated both analytically and via simulations that the diversity order of the space–time coded UWB system can be increased. These seemingly contradictory results can be explained by the fact that the diversity order is generally helpful in achieving better BER performance in the high SNR regime, while the UWB systems are required to operate in the low SNR range. Thus the diversity order pointed out in [82] is beneficial only in the high SNR regime. The simulation results illustrated in Fig. 10 give a quantitative description for this idea.

In the following, we will briefly introduce the approach of [82]. Afterwards, further performance investigation will be conducted.

Let $w(t)$ be the waveform of the monopulse used to carry information in a UWB system. Its duration T_w is typically between 0.2–2 ns. The energy carried by $w(t)$ is normalized, i.e., $\int_0^{T_w} w^2(t)dt = 1$. The information symbol $\mathcal{S}$ can be conveyed by N_f pulses

$$s(t) = \sum_{n_f=0}^{N_f-1} a_{n_f}(\mathcal{S}) w\left(t - n_f T_f - b_{n_f}(\mathcal{S})\Delta\right) \tag{18}$$

where $a_{n_f}(\mathcal{S})$ and $b_{n_f}(\mathcal{S})$ are the functions of both information symbol $\mathcal{S}$ and frame index n_f; Δ is the position modulation index; T_f is the frame duration; and $s(t)$ is the signal to be transmitted. Here we consider the case of only one user. If multiple users are considered, either the amplitude or the position of the pulse can be further changed, but independently from the information symbol $\mathcal{S}$, using an appropriate spreading code. If $a_{n_f}(\mathcal{S}) = 1$ for all $n_f \in [0, N_f - 1]$, (18) implies a PPM; on the other hand, it implies a PAM if $b_{n_f}(\mathcal{S}) = 0$ for all $n_f \in [0, N_f - 1]$.

A general assumption for STC is that the channel fading will not change for some period. Here we maintain this assumption, i.e., the channel fading will not change in N_f and $2N_f$ consecutive encoding frames, respectively, for the two encoding schemes addressed below.

Now let us consider the case of two transmit antennas and one receive antenna. In [82], two space–time coding schemes are proposed for this case.

A. The 1S/2A Coding Scheme

In this scheme, one information symbol $\mathcal{S}$ is transmitted simultaneously from the two transmit antennas. The signals to be transmitted at antennas numbered with 0 and 1 are as follows, respectively:

$$\begin{cases} s_0(t) = \sqrt{\frac{E_0}{2N_f}} \sum_{n_f=0}^{N_f-1} (-1)^{n_f} \mathcal{S} w(t - n_f T_f) \\ s_1(t) = \sqrt{\frac{E_0}{2N_f}} \sum_{n_f=0}^{N_f-1} \mathcal{S} w(t - n_f T_f) \end{cases} \tag{19}$$

where E_0 is the relative symbol energy, i.e., $\int_0^{N_f T_f} s_0^2(t)dt = \int_0^{N_f T_f} s_1^2(t)dt = E_0/2$. It is easy to cast (19) into the form of (18). Since one symbol is encoded across two antennas per N_f frames in this coding scheme, we call it the 1S/2A coding scheme.

The schematic diagram for the decoding system is illustrated in Fig. 8.

As shown in Fig. 8, the whole decoding system is divided into four steps. First, the received signal $r(t)$ passes through a matching filter whose impulse response is $w(-t)$ and the sampled [with sampling rate being $1/(2T_w)$] signal is divided into two branches: evenly indexed frame, denoted as $x_e(l)$; and oddly indexed frame, denoted as $x_o(l)$, respectively. Secondly, the signals $x_e(l)$ and $x_o(l)$ are fed to

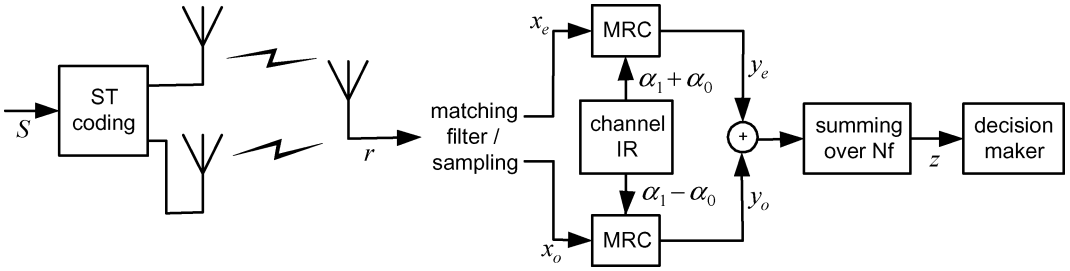

Fig. 8. *The schematic diagram for space–time encoding–decoding scheme 1S/2A.*

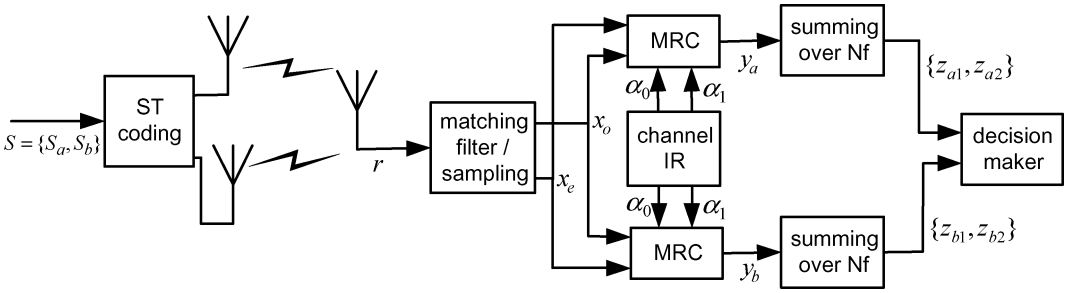

Fig. 9. *The schematic diagram for space–time encoding–decoding scheme 2S/2A.*

the Rake receiver (with L fingers) and combined with the maximum ratio combining (MRC) algorithm, producing signals $y_e(n_f)$ and $y_o(n_f)$, respectively. Thirdly, the signals $y_e(n_f)$ and $y_o(n_f)$ are summed up over the N_f frames corresponding to the same symbol $\mathcal{S}$, producing signal z. It is in this step that the SNR is strengthened due to spatial processing. Finally, the signal z is fed to the decision maker to decode the symbol $\mathcal{S}$.

B. The 2S/2A Coding Scheme

In this scheme, two information symbols $\mathcal{S}_a$ and $\mathcal{S}_b$ are transmitted simultaneously from the two transmit antennas but encoded across two consecutive frames in the following way [82]:[4]

$$\begin{cases} s_0(t) = \sqrt{\frac{E_0}{4N_f}} \sum_{n_f=0}^{N_f-1} \big[\mathcal{S}_a w(t-2n_fT_f) \\ \qquad\qquad - \mathcal{S}_b w(t-2n_fT_f-T_f)\big] \\ s_1(t) = \sqrt{\frac{E_0}{4N_f}} \sum_{n_f=0}^{N_f-1} \big[\mathcal{S}_b w(t-2n_fT_f) \\ \qquad\qquad + \mathcal{S}_a w(t-2n_fT_f-T_f)\big]. \end{cases} \tag{20}$$

It can be also shown that (20) can be cast into the form of (18). Since two symbols are simultaneously encoded across two antennas per N_f frames in this coding scheme, we call it the 2S/2A coding scheme.

The schematic diagram for the encoding–decoding system is illustrated in Fig. 9.

As shown in Fig. 9, the whole decoding system is divided into five steps. First, the received signal $r(t)$ passes through a matching filter whose impulse response is $w(-t)$; the sampled [with sampling rate being $1/(2T_w)$] signal in the first N_f frames is divided into two branches: evenly indexed frame, denoted as $x_e(l)$, and oddly indexed frame, denoted as $x_o(l)$, respectively. Secondly, the signals $x_e(l)$ and $x_o(l)$ are fed to the Rake receiver (with L fingers) and combined with the MRC algorithm, producing signals $y_a(n_f)$ and $y_b(n_f)$, respectively. Thirdly, $y_a(n_f)$ and $y_b(n_f)$ are summed up, respectively, over the first N_f frames, producing signals z_{a1} and z_{b1}. Fourthly, the same procedure as in the previous three steps is repeated for the second N_f frames, producing signals z_{a2} and z_{b2}, respectively. Sum up signals z_{a1} and z_{a2}, z_{b1} and z_{b2} respectively, yielding the signals z_a and z_b. Finally, the signals z_a and z_b are fed to the decision maker to decode the symbols $\mathcal{S}_a$ and $\mathcal{S}_b$.

The receiver processing details for the two schemes can be found in [82]. In the above schemes, the inherent diversity of UWB signals in the temporal domain is collected by the Rake, while the diversity in the spatial domain is harvested by the use of the space–time coding.

C. Simulation Results

The performance of the aforementioned space–time coding schemes is illustrated in Fig. 10. In the simulation,

[4]Note that the scaling coefficient $\sqrt{E_0/4N_f}$ is different from that in [82]. We choose the scaling coefficient as shown here in order to make the energy consumption per symbol per frame be the same as that for the 1S/2A scheme.

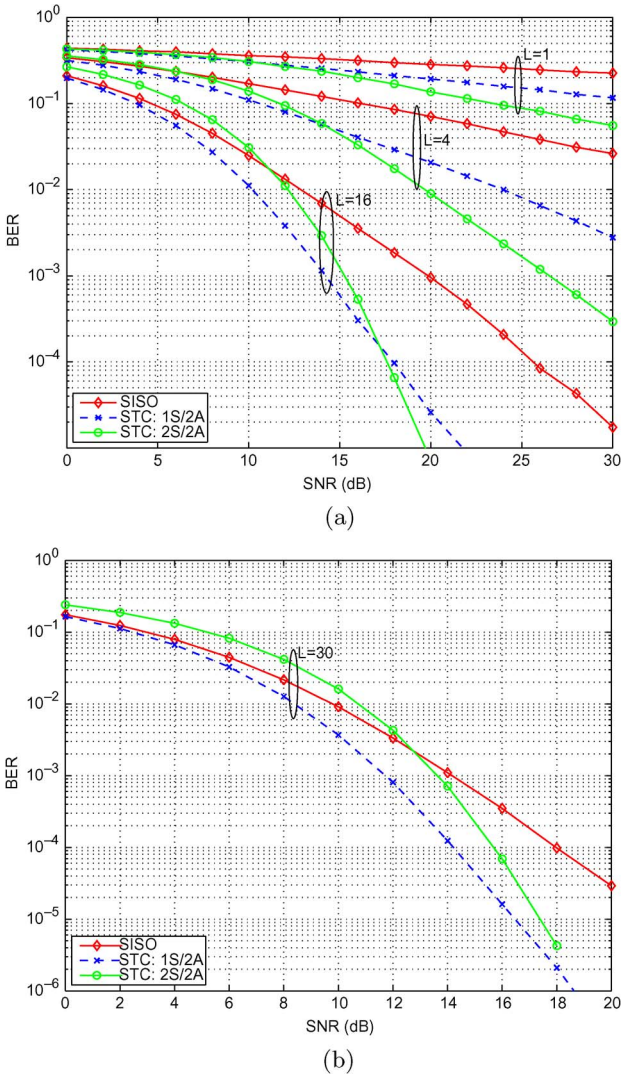

Fig. 10. ***BER performance comparison of SISO and MISO with space–time coding schemes 1S/2A and 2S/2A.***

the standard UWB channel model [28], [47] is used, where the exponentially decaying parameters of the power delay profile for clusters and rays are chosen as 33 and 5 ns, respectively, and the cluster arrival rate and ray arrival rate are set to be 0.5 $(\text{ns})^{-1}$ and 2 $(\text{ns})^{-1}$, respectively [82]. The sampling period is chosen as 0.7 ns. N_f is set to be two. The second derivative of the Gaussian function is chosen as the information carrying monopulse, i.e.,

$$w(t) = c_{\text{norm}}\left[1 - 4\pi\left(\frac{t}{\tau_p}\right)^2\right]\exp\left[-2\pi\left(\frac{t}{\tau_p}\right)^2\right] \quad (21)$$

where the constant c_{norm} is to normalize the energy of the pulse $w(t)$ and $\tau_p = 0.1225$ ns. The autocorrelation $R_w(\tau)$ of $w(t)$ is given by [33]

$$R_w(\tau) = c_{\text{norm}}\left[1 - 4\pi\left(\frac{\tau}{\tau_p}\right)^2 + \frac{4\pi^2}{3}\left(\frac{\tau}{\tau_p}\right)^4\right] \times \exp\left[-\pi\left(\frac{\tau}{\tau_p}\right)^2\right].$$

From Fig. 10, it can be observed that the 1S/2A scheme outperforms the SISO systems in BER performance according to per symbol per frame per unit energy data transmission, while the 2S/2A scheme outperforms considerably both the 1S/2A scheme and SISO in the BER performance when the SNR is high, but yields (marginally or moderately) poorer BER performance than both the 1S/2A scheme and SISO when the SNR is low. Note that the 2S/2A scheme requires the longest decoding delay among the three kinds of systems. Notice also that the range of aforementioned low and high SNR depends on

Table 1 Performance Comparison Among the SISO, 1S/2A, and 2S/2A Schemes

	energy consumption per N_f frames	symbol rate per N_f frames	decoding delay	BER
SISO	$E_0 N_f$	N_f symbols	1 frame	$> \text{BER}_{1S/2A}$ $< \text{BER}_{2S/2A}$ at low SNR $> \text{BER}_{2S/2A}$ at high SNR
1S/2A scheme	E_0	1 symbol	N_f frames	$< \text{BER}_{\text{SISO}}$ $< \text{BER}_{2S/2A}$ at low SNR $> \text{BER}_{2S/2A}$ at high SNR
2S/2A scheme	E_0	1 symbols	$2N_f$ frames	$> \text{BER}_{\text{SISO}}$ at low SNR $< \text{BER}_{\text{SISO}}$ at high SNR $> \text{BER}_{1S/2A}$ at low SNR $< \text{BER}_{1S/2A}$ at high SNR

the number of fingers in the Rake receiver. Table 1 gives a detailed comparison among the SISO, 1S/2A, and 2S/2A schemes in terms of data rate, energy consumption, and BER performance.

Therefore, we recommend to use the 1S/2A coding scheme if the number of fingers in the Rake receiver is not too large, say, less than 16, considering both the BER performance and decoding delay.

From Fig. 10 and the channel capacity for the MISO case (Fig. 1), we can draw a basic conclusion about the diversity and system performance: if the available SNR is too low, it is better to concentrate the available power on a single antenna or a single symbol to transmit the information data than to distribute the power across multiple antennas or symbols to gain diversity; the diversity gain can only be realized if the available SNR is sufficiently high. In other words, the transmit power should be somewhat peaky (in the sense addressed in [52] and [72]) if the available SNR is too low. The reason behind this fundamental compromise can be deduced from an extreme case where the available SNR is so low that we cannot correctly receive one single bit in a given period if we distribute the low energy across multiple antennas or symbols, while we can correctly receive several bits in the given period if we use only one antenna or spend the whole power on one single symbol to transmit. In practice, it is important to give some quantitative characterization for this fundamental compromise such as the critical transmission rate given in the preceding section. Unfortunately, it seems not easy to provide such a quantitative characterization for the space–time coding schemes discussed here. We can just state that it depends on the channel length L, the channel fading parameters, and the STC schemes.

D. Performance of Antenna Selection

The gains obtained by deploying multiple antennas come at the price of hardware complexity. The radio front end has a complexity, size, and cost that scale with the number of antennas [61]. A possible way to reduce the cost and complexity while not sacrificing the gains too much is to use antenna selection schemes. For narrow-band MIMO communications systems, there are many research results about antenna selection; see the comprehensive surveys [50], [61] and references therein. However, for UWB-MIMO systems, few results are currently available.

A general setup of the antenna selection is to choose $\bar{N}_T$ transmit and $\bar{N}_R$ receive antennas out of N_T transmit and N_R receive antennas, respectively. For a fixed $\bar{N}_T$ and $\bar{N}_R$, the selection is normally based on two kinds of performance criteria, which are either the BER performance or the channel capacity [61]. Generally, the selection based on the BER performance will coincide with the selection based on the received SNR. On the other hand, the selections based on the BER performance and channel capacity, respectively, do not agree with each other. As shown in [51] for narrow-band MIMO, only 50% of selections based on the two criteria in all the fading channel realizations agree with each other.

In the extreme case when $\bar{N}_T$ is not fixed in advance and $\bar{N}_R = N_R$, the selection based on the channel capacity will yield the water-filling algorithm across the frequency-spatial domain [86]. The transmit power will be distributed in patches on the surface of the frequency and spatial domains. Thus in a certain frequency band, only some of the antennas are selected for transmission. As shown in Fig. 6, this kind of antenna selection can yield considerable gains in capacity in the low SNR range. However, if antenna selection is based only on the spatial domain, whether or not the selection can yield performance gain will be determined by the scattering environments and the relative locations of the antennas.

Currently, there are no reports to address the antenna selection problem for UWB-MIMO systems in the sense of aforementioned general setup. In the following, let us consider the simple case where $N_T = 2$ and $N_R = 1$. Therefore, we have $\bar{N}_T = \bar{N}_R = 1$. In this case, antenna selection actually reduces to antenna switching. As mentioned, it was pointed out in [76] that antenna switching in multiple transmit antenna systems does not provide diversity gain in the strict sense. Examining the simulation scenario investigated in [76], the two channels from the transmitters to the receiver experience the same scattering environment and thus possess the same pdf in their fading statistics. Generally, the spatial diversity exists for rich scattering environments and sufficiently separated antennas for narrow-band systems, and antenna selection can be used to exploit such kind of diversity even though the channels possess the same fading pdf. For UWB-MIMO channels, the fading is distributed over many channel taps and the Rake receiver is normally used to collect the received energy across these taps. Even though every channel tap may experience fading, and spatial diversity may exist among these single taps for different channels, the Rake receiver actually smooths the fading by the (possibly weighted) summation of the signals from the selected channel taps. Therefore, antenna selection will not yield diversity gain in the strict sense if the spatial channels share the same fading pdf. On the other hand, if the antennas are separated sufficiently far, different scattering environments may be experienced by the spatial channels. For example, when one channel is in line-of-sight (LOS) and another channel is in non-LOS (NLOS), the channels will have different fading pdfs (in either forms or parameters) and different power delay profiles. In such a scenario, the spatial diversity exists even after the Rake processing, and antenna selection can be used to improve the system performance.

To illustrate the above idea, let us consider the following experiment. There are two transmit antennas and one receive antenna in a typical office environment, with one transmit antenna in LOS and another in NLOS, as shown in Fig. 11(a). All the antennas are omnidirectional

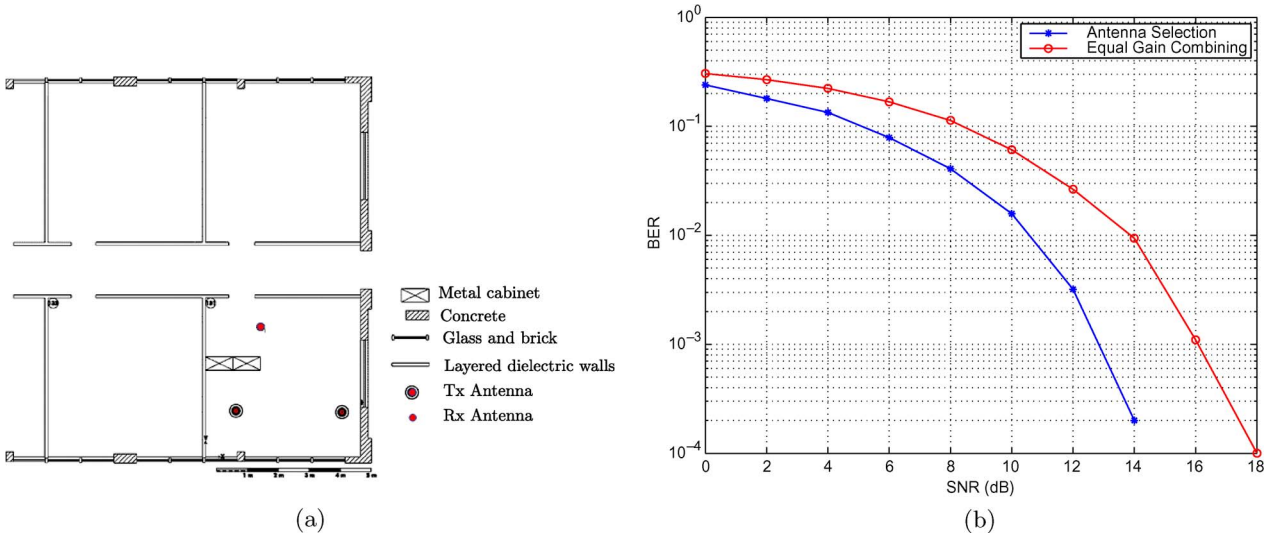

Fig. 11. ***Performance comparison between antenna selection and equal gain combiner. (a) Floor plan and (b) BER performance.***

UWB conical antennas with 3 dB gain. The height of the room is 3.02 m, and the height of transmit and receive antennas is 1.5 m above ground. The channel transfer functions between the receiver and each transmitter are measured at the sampled frequencies from 1 to 11 GHz with frequency sampling step of $\Delta f = 6.25$ MHz (so 1602 frequency points are measured for each channel). The channel impulse responses (CIRs) from each transmitter to the receiver are obtained by the inverse Fourier transform of the corresponding channel transfer functions. The binary PPM is used to transmit the information symbols and selective Rake (SRake) [56], [78] receiver with the ten strongest taps being selected to collect the signal energy. Two kinds of receivers are compared. The first is based on the antenna selection scheme, where one of the transmit antennas from which the receiver receives stronger summation signal in the SRake is selected for symbol transmission. The second is based on an equal gain combining receiver, where both transmitters are used to transmit symbols. Note that in the second case, the symbol energy per transmit antenna is halved as that in the first case. The performance comparison for the two cases is illustrated in Fig. 11(b). It is seen that the antenna selection can provide better BER performance than the equal gain combiner.

The reason for the above phenomenon is that the two channels exhibit some kind of diversity. To have a deep insight into this phenomenon, let us return to the general UWB channel model proposed in [47, Appendix A]. There are two kinds of fadings in the CIR, with one characterizing the small-scale fading for each channel tap and another the large-scale shadowing, which applies to all the channel taps. Clearly, the spatial diversity among the channels in UWB-MIMO systems is characterized by the large-scale shadowing, while the temporal diversity among the taps of each single channel is characterized by the small-scale fading. Generally, the Rake receivers can remove the micro diversity caused by the small-scale fading, but they cannot remove the macro diversity caused by the large-scale shadowing if the shadowing statistics are different.

IV. UWB BEAMFORMING

Array processing and smart antenna concepts offer a promising solution to the significant increasing of data rates in wireless transmission systems. There has been widespread interest in array processing over more than four decades, especially in radar and deep-space exploration, while the interest in the application of array processing in wireless communication systems started two decades ago and booms rapidly nowadays. Perhaps the delayed surging of interest in the latter field is due to, on one hand, lack of the need for the array technology in wireless communication market (imagine that wireless communications have become popular only in the recent two decades) and, on the other hand, the difficulty in dealing with multipaths of the propagation signals in wireless communications, which will cause fundamental trouble for the array processing.

Beamforming for UWB impulse signals has some special properties that are quite different from the narrow-band beamformers. For example, the use of unequal weighting filters for the individual antenna branch will increase the side-lobe level in UWB beamforming, and there are no grating lobes in the UWB beampattern [60]. In this section, we will investigate how these properties appear in UWB beamformers.

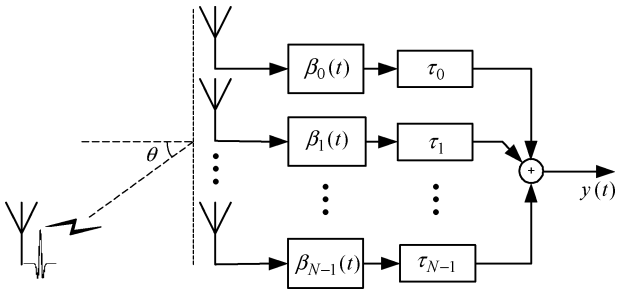

Fig. 12. *The schematic diagram for an ideal UWB impulse beamforming system.*

A. Ideal UWB Impulse Beamforming

An ideal UWB impulse beamforming system is illustrated in Fig. 12, where N receive antennas are aligned linearly and identically separated by a distance d, which is several centimeters in typical usage. All the antennas are assumed to be omnidirectional. As in the narrow-band case, we assume that the receive antenna array is located in the far field, i.e., the distances from the transmit antenna to each receive antenna are much larger than d, so that the rays from the transmit antenna to each receive antenna can be considered parallel to each other. In Fig. 12, $\beta_i(t)$, $i = 0, \ldots, N-1$, are the impulse responses of the prefilters, and τ_i, $i = 0, \ldots, N-1$, are the additional time delays, which are applied to each branch to control the steering direction of the beamformer.

Let c be the propagation speed of the UWB impulse wave, θ the angle between the incidence ray and broadside direction of the antenna array, and $x(t)$ the transmitted signal. Generally, $x(t)$ is a train of monopulses,[5] i.e.,

$$x(t) = \sum_{n=-\infty}^{+\infty} w(t - nT_f) \tag{22}$$

where $w(t)$ is the waveform of UWB monopulse and T_f is the pulse repetition period. The output of the beamformer can be expressed as

$$y(t;\theta) = \sum_{k=0}^{N-1} y_k(t - \tau_k)$$
$$y_k(t) = x\left(t - k\frac{d}{c}\sin\theta\right) * \beta_k(t), \quad k = 0, \ldots, N-1$$

where $*$ denotes the convolution. For the case of $\beta_k(t) = (1/N)\delta(t)$ (i.e., constant and equal weighting), $\tau_k = (k-1)\Delta\tau$ ($\Delta\tau$ is a constant), and $w(t)$ is as given in (21), the output $y(t;\theta)$ is shown in Fig. 13. From this figure, we can see that:

- the main power of the beamformer output is focused on a certain direction;
- the focused direction can be controlled by adjusting the time delays τ_i, $i = 0, \ldots, N-1$.

Now we consider the beampattern problem, which is a key issue for a beamformer. In the literature, there are three types of definitions for the beampattern [60].

Type I

$$BP_I(\theta) = \frac{\int_{-\infty}^{+\infty} |y(t;\theta)|^2 dt}{\int_{-\infty}^{+\infty} |x(t)|^2 dt}. \tag{23}$$

Type II

$$BP_{II}(\theta) = \frac{\max\limits_{t\in(-\infty,+\infty)} |y(t;\theta)|^2}{\max\limits_{t\in(-\infty,+\infty)} |x(t)|^2}. \tag{24}$$

Type III

$$BP_{III}(\theta) = \frac{\max\limits_{t\in(-\infty,+\infty)} \int_{t-T/2}^{t+T/2} |y(t;\theta)|^2 dt}{\max\limits_{t\in(-\infty,+\infty)} \int_{t-T/2}^{t+T/2} |x(t)|^2 dt}. \tag{25}$$

In using the above definitions, a monopulse, instead of a train of monopulses, should be adopted in (22) to avoid the trivial singularity.

For narrow-band beamformers, the three kinds of definitions for the beampattern are equivalent, but for UWB, these definitions give different results. Clearly, definition (25) reduces to (23) when T approaches infinity, and (25) reduces to (24) when T approaches zero. Therefore, (25) gives a more general definition. In general, (23) is more suitable for theoretical analysis, while (25) is more convenient for practical beampattern calculation. For the case shown in Fig. 13, the corresponding beampattern is illustrated in Fig. 14.

B. The Main Lobe Beamwidth of UWB Beamformers

It is difficult to calculate the beamwidth of the main lobe of a UWB beamformer according to (23), (24), or (25) because of the complexity of the UWB waveform. This is different from the narrow-band case. In this section, we will give a coarse estimation for the main-lobe beamwidth for the UWB beamformer.

[5]Notice that the interframe coding is not considered in this section, as is usual for the beamforming problem.

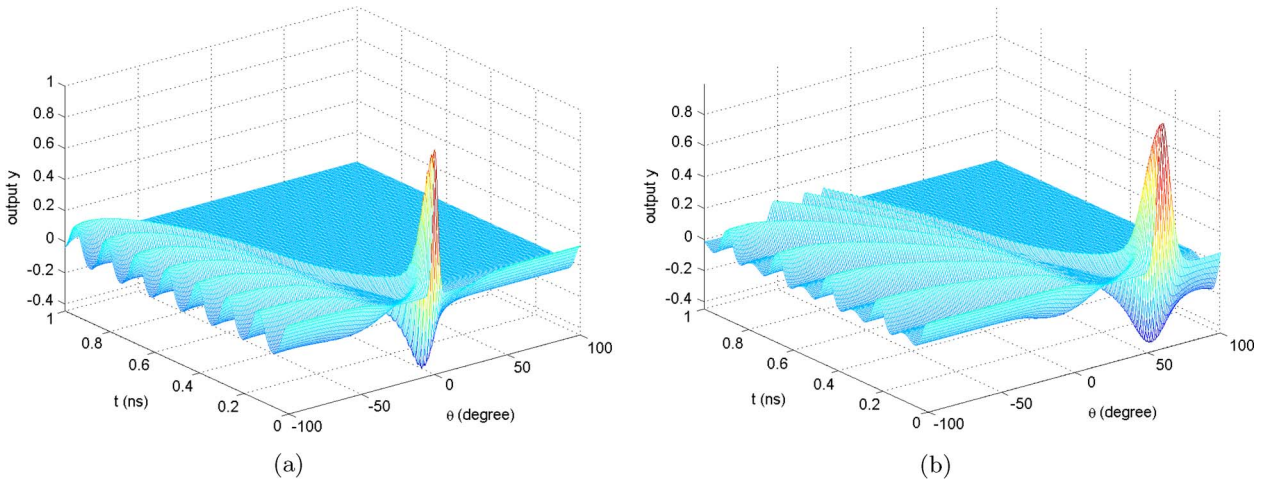

Fig. 13. ***Beamformer output as a function of time and spatial angle, where N = 8, d = 3.63 cm, τ_p = 0.1225 ns. (a) $\Delta\tau$ = 0 and (b) $\Delta\tau$ = 0.1052 ns.***

To address this problem, we assume that $\beta_k(t) = \delta(t)$, $\Delta\tau = 0$, and N is sufficiently large. Let T_w denote the duration of the UWB impulse. Let E_w be the energy of the monopulse $w(t)$. First, consider the case that the UWB impulse signal arrives from the broadside of the array (i.e., $\theta = 0$). In this case, all the signals from each array branch will arrive at the same time, resulting in a coherent summing up and producing a maximum output. Thus we have

$$\int_{-\infty}^{+\infty} |y(t;0)|^2 dt = N^2 E_w, \quad \text{and} \quad BP_I(\theta) = N^2.$$

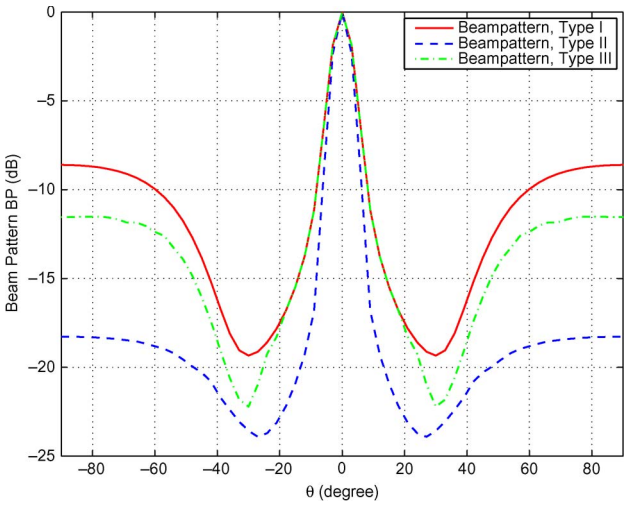

Fig. 14. ***Illustration of three types of beampattern, where N = 8, d = 3.63 cm, τ_p = 0.1225 ns, and T = 0.2419 ns.***

Now suppose the signal ray arrives from the direction of some angle $\theta_{-3\text{ dB}}$ such that $N/\sqrt{2}$ pulses are contained in the time window of duration T_w. Then we have

$$\int_{-\infty}^{+\infty} |y(t;0)|^2 dt \approx \frac{N^2}{2} E_w, \quad \text{and} \quad BP_I(\theta_{-3\text{ dB}}) \approx \frac{N^2}{2}.$$

Therefore, the beamwidth of the main lobe of the beamformer, denoted as θ_{bw}, is $2\theta_{-3\text{ dB}}$. The corresponding $\theta_{-3\text{ dB}}$ angle is related to other parameters of the beamformer as follows:

$$\frac{N}{\sqrt{2}} \cdot \frac{d}{c} \sin\theta_{-3\text{ dB}} = T_w$$

which gives

$$\theta_{bw} = 2\theta_{-3\text{ dB}} = 2\arcsin\frac{\sqrt{2}cT_w}{Nd}. \tag{26}$$

For the case in Fig. 14, if we choose T_w as the width between the two points at which $w(t)$ is across zero ($T_w = 0.0691$ ns), (26) gives $\theta_{bw} = 11.6°$, which is quite congruous with the numerical result.

C. Optimal Beamforming

In the preceding section, we derived the beamwidth for the main lobe under the condition that all the branches in the array are equally weighted. In this section, we will explain the reason for making such a choice. Now let us

consider the general setup of the beamformer illustrated in Fig. 12. Assume that all the weighting functions $\beta_k(t)$ are also of short duration, i.e., $\beta_k(t) = 0$ for all $|t| \geq T_\beta$ and $k \in \{0, 1, \ldots, N-1\}$. For the convenience of discussion, we assume that $T_\beta \leq T_w$. It is also assumed in this section that $\tau_k = 0, \forall k \in \{0, 1, \ldots, N-1\}$, and only a monopulse is adopted in the transmitted signal, i.e., $x(t) = w(t)$. Similar to the argument in the preceding section, we can conclude that the main lobe is obtained when $\theta = 0$. Hence the strength of the main lobe is

$$BP_{ml} = BP_I(0) = \frac{1}{E_w}\int_{-\infty}^{+\infty} |y(t;0)|^2 dt = \frac{1}{E_w}\int_{-\infty}^{+\infty}\left[\sum_{k=0}^{N-1} w(t) * \beta_k(t)\right]^2 dt.$$

For the side lobe to appear, the ray incidence angle should be wide enough such that the two pulses from two adjacent branches are separated. This happens if

$$\frac{d}{c}\sin\theta \geq T_w + T_\beta. \tag{27}$$

Because of the equidistance property in the array, the pulses from all the branches will be separated from each other in the time domain if the above condition holds. Thus the strength of the side lobes reads as

$$BP_{sl}(\theta) = BP_I(\theta) = \frac{1}{E_w}\int_{-\infty}^{+\infty} |y(t;\theta)|^2 dt = \frac{1}{E_w}\sum_{k=0}^{N-1}\int_{-\infty}^{+\infty}\left[w\left(t - k\frac{d}{c}\sin\theta\right) * \beta_k(t)\right]^2 dt.$$

A general design objective for a beamformer is to maximize the strength of the main lobe while minimizing the strength of the side lobes simultaneously. This objective can be mathematically formulated as

$$\begin{cases} \max_{\beta_k(t), k=0,\ldots,N-1} BP_{ml} \\ \quad = \int_{-\infty}^{+\infty}\left[\sum_{k=0}^{N-1} w(t) * \beta_k(t)\right]^2 dt \\ \text{such that} \quad BP_{sl}(\theta) \\ \quad = \sum_{k=0}^{N-1}\int_{-\infty}^{+\infty}\left[w\left(t - k\frac{d}{c}\sin\theta\right) * \beta_k(t)\right]^2 dt \leq 1. \end{cases} \tag{28}$$

The above criterion is equivalent to maximizing the ratio $BP_{ml}/BP_{sl}(\theta)$.

About this problem, we have the following proposition.

Proposition 1: Suppose the weighting filters $\beta_k(t)$, $k = 0, \ldots, N-1$, are of short duration. The optimal beamformer is obtained if all the weighting filters $\beta_k(t)$ are identical. For the optimal beamformer, the amplitude of the side lobe is independent of the ray incidence angle θ if (27) is satisfied, and the ratio between the amplitude of the main lobe and side lobes is

$$\frac{BP_{ml}}{BP_{sl}(\theta)} = N.$$

The proof of the proposition is provided in the Appendix. It is easy to understand the result in Proposition 1. Notice that all the weighting filters $\beta_k(t)$ $(k = 0, 1, \ldots, N-1)$ play an equal role in the optimization problem (28). Because of this symmetry, the solution to the problem (28) will be that all the weighting filters are in the same form. A less obvious observation is as follows. Suppose all the weighting filters are equal before the time instant under consideration. Now we start to increase the value of a given weighting filter. Then the increased value in this weighting filter will contribute more to the side lobes than to the main lobe of the beamformer.

D. Various Aspects of UWB Beamformers

Similar to the narrow-band case, UWB beamformers can be used for both estimation of direction of arrival (DOA) of UWB rays and beam steering for UWB communications.

For beam steering, suppose that the steering angle is θ_0. Then $\Delta\tau$ should be chosen such that

$$\Delta\tau = \frac{d}{c}\sin(\theta_0).$$

For DOA estimation, the procedure is quite different from the narrow-band case. To address this issue, let us investigate the beamformer output in more detail. This is illustrated in Fig. 15, where we fix the beam steering angle, which is controlled by $\Delta\tau$, and investigate the beamformer output from the viewpoint of impinging angle and time, respectively. Denote now the beam steering angle as θ_{DOA}, which is also called look direction. From Fig. 15(a), we can see that the levels of the beamformer output for different impinging angles are almost identical when the steering angle deviates from the impinging angle by some amount. This kind of relationship between θ and y excludes the possibility of solving θ directly from $y(t;\theta)$. From Fig. 13(b), we can see that the difference among the time-patterns for different look directions is also marginal

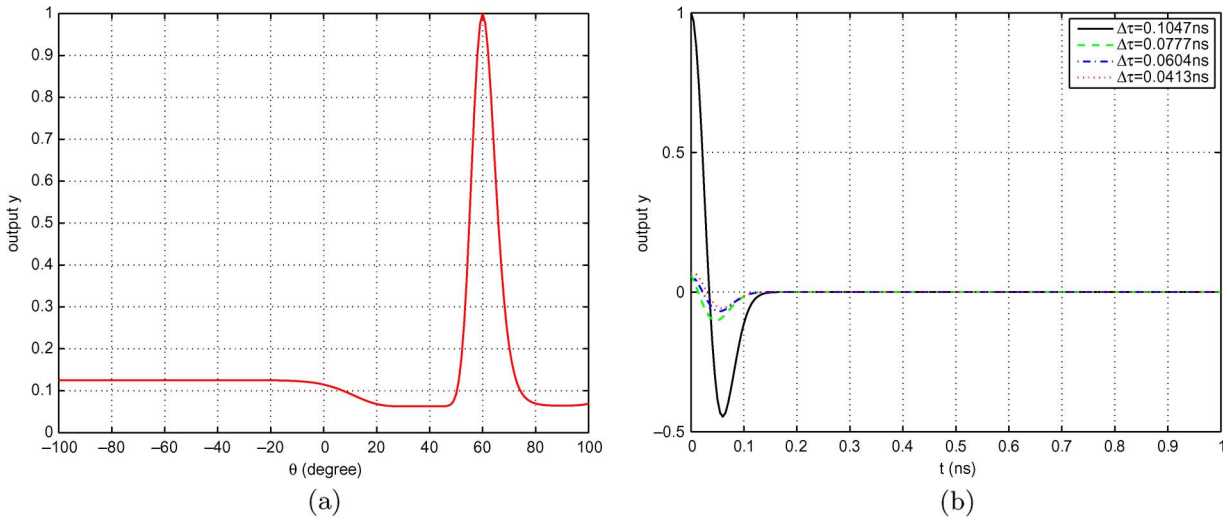

Fig. 15. *Beamformer output for the purpose of DOA estimation: (a) impinging angle-pattern for a fixed look direction θ_{DOA}, where $t = 0$ and $\Delta\tau = 0.1047$ ns, implying $\theta_{\mathrm{DOA}} = 60^\circ$; (b) time-pattern for four different fixed look directions θ_{DOA}, where $\theta = 60^\circ$ and $\Delta\tau = 0.1047, 0.0777, 0.0604,$ and 0.0413 ns, implying $\theta_{\mathrm{DOA}} = 60^\circ, 40^\circ, 30^\circ,$ and 20°, respectively.*

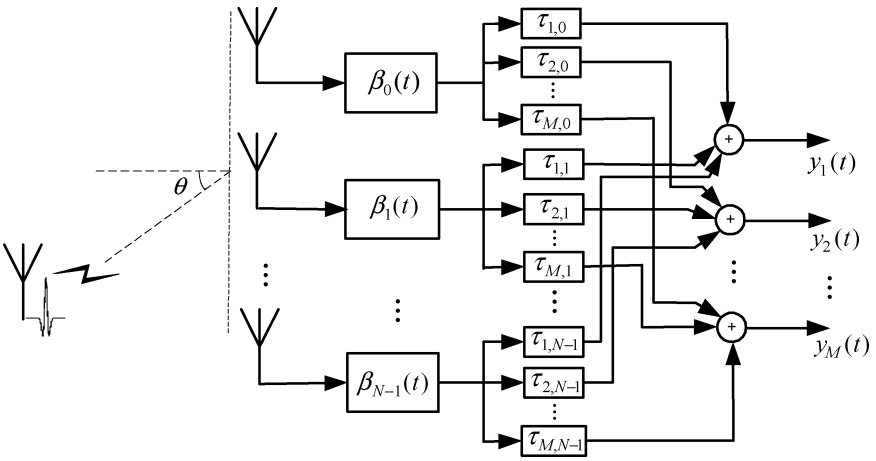

Fig. 16. *The schematic diagram for DOA estimation using UWB beamformer.*

when the look direction is not locked in some range of the impinging angle. This also weakens the possibility of solving θ from the history of $y(t;\theta)$, $t \in [t_0, t_1]$, where t_0 and t_1 are two given observation time instants.

To solve the above problem, a DOA estimation approach is shown in Fig. 16.

In Fig. 16, there are M outputs, each of which aims to find a direction with the help of the time delay vector $[\tau_{i,0}, \tau_{i,1}, \ldots, \tau_{i,N-1}] = \Delta\tau_i[0, 1, \ldots, N-1]$, $i = 1, 2, \ldots, M$. Therefore, if the ith output is maximum among all $\{y_1, \ldots, y_M\}$, the DOA of the incidence ray will read as

$$\theta_{\mathrm{DOA}} = \arcsin\frac{c\Delta\tau_i}{d}.$$

The design of the difference between $\Delta\tau_i$ and $\Delta\tau_j$, $i \neq j$, depends on the resolution requirement for DOA estimation and system complexity. However, the following relationship:

$$\min_{j=1,\ldots,M, j\neq i}\left|\arcsin\frac{c\Delta\tau_i}{d} - \arcsin\frac{c\Delta\tau_j}{d}\right| \leq \theta_{bw}, \quad \forall i \in \{1, \ldots, M\}$$

should be satisfied. Otherwise, it is possible that all the outputs will produce small signals of almost equal amplitude, resulting in a failure to find the DOA.

Noticing that the delays among different branches in Fig. 16 are fixed and well structured, the M outputs in one

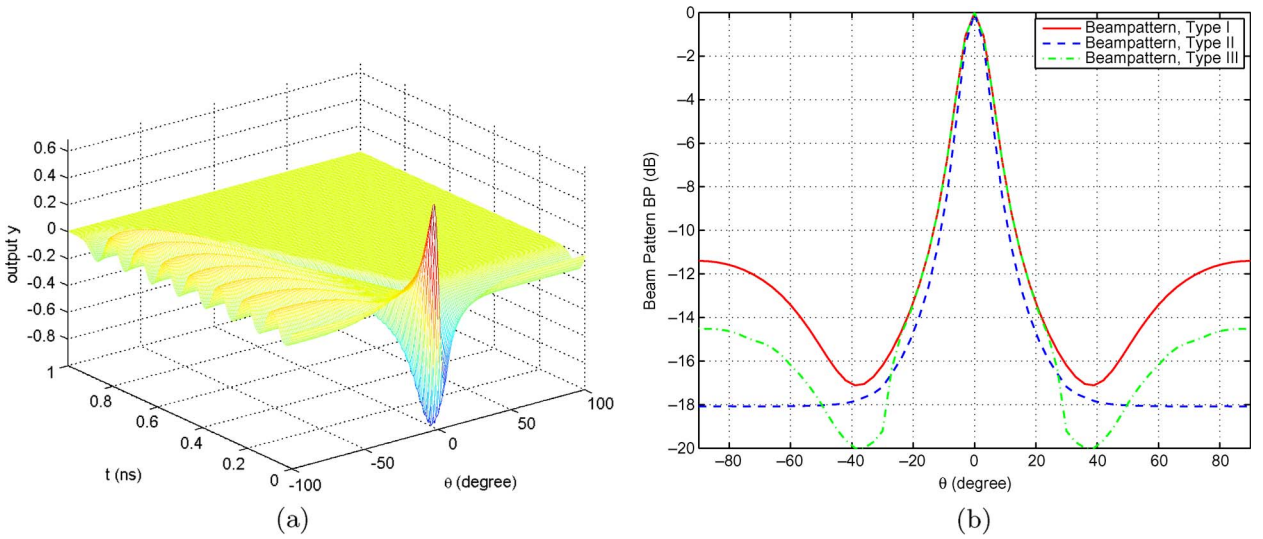

Fig. 17. ***The space–time response and beam pattern of the beamformer using the first derivative of the Gaussian monopulse, where $\tau_p = 0.1225$ ns, $N = 8$, $d = 3.63$ cm, and $\Delta\tau = 0$. (a) Space–time response and (b) beam pattern.***

antenna branch can be realized by one chip using an analog radio-frequency (RF) domain finite impulse response (FIR) filter as proposed in [53], [54], and [66]. This technology will make the beamformer in Fig. 16 less expensive to implement. If the delays in Fig. 16 could be electronically adjusted as changing the phase of the signals for the case of narrow-band beamformers, it would be possible to further simplify the architecture illustrated in Fig. 16, but it seems difficult to use the current technology to electronically adjust the delay.

For the element distance, there is a limit for the maximal distance if interframe coding, which is often used in UWB systems as illustrated in Section III, is adopted in the transmitted signal. In this case, to avoid catastrophic superposition of the signals coming from different frames, the distance between two nearest elements d should be chosen such that

$$d \leq cT_f.$$

In order to implement the beamformer mentioned in Fig. 15, one should be able to adjust the delay between the pulse trains in the order of several tens of picosecond. Currently, the arbitrary waveform generator (AWG) available in the market, e.g., AWG7102 by Tektronix,[6] can be used to generate two pulse trains with adjustable delay between each other in 100 ps. Using an analog radio-frequency domain FIR filter proposed in [53], [54], and [66] is another possibility to realize the required delay.

In UWB communication systems, other kinds of monopulses are also adopted. A popularly used form is the first derivative of the Gaussian monopulse

$$w(t) = c'_{\text{norm}}\, t \exp\left[-2\pi\left(\frac{t}{\tau_p}\right)^2\right]$$

where the constant c'_{norm} is to normalize the peak amplitude of the pulse $w(t)$. The space–time response and beam pattern of the beamformer are illustrated in Fig. 17.

Another kind of less popular but interesting monopulse is proposed by Hussain [34], [35]

$$w(t) = \frac{1}{1-\xi}\left\{\exp\left[-4\pi\left(\frac{t}{\tau_p}\right)^2\right] - \exp\left[-4\pi\left(\frac{\xi t}{\tau_p}\right)^2\right]\right\}, \quad \xi \neq 1 \quad (29)$$

where ξ is a scaling parameter and τ_p is to control the spread-in-time of the monopulse, as for the case of the Gaussian monopulse. The space–time response and beam pattern of the beamformer are illustrated in Fig. 18.

V. TESTBED RESULTS

Testbeds give a fundamental insight into the practical aspects of a developed approach and provide an important tool to verify the results of a model-based system design. In order to simplify the access to the real UWB-MIMO channel, a universal offline testbed with a MatLab interface and very high data rate (VHDR) MIMO multiband-OFDM (MB-OFDM) system-simulator was set

[6]http://www.tek.com/site/ps/0,,76-19779-INTRO_EN,00.html.

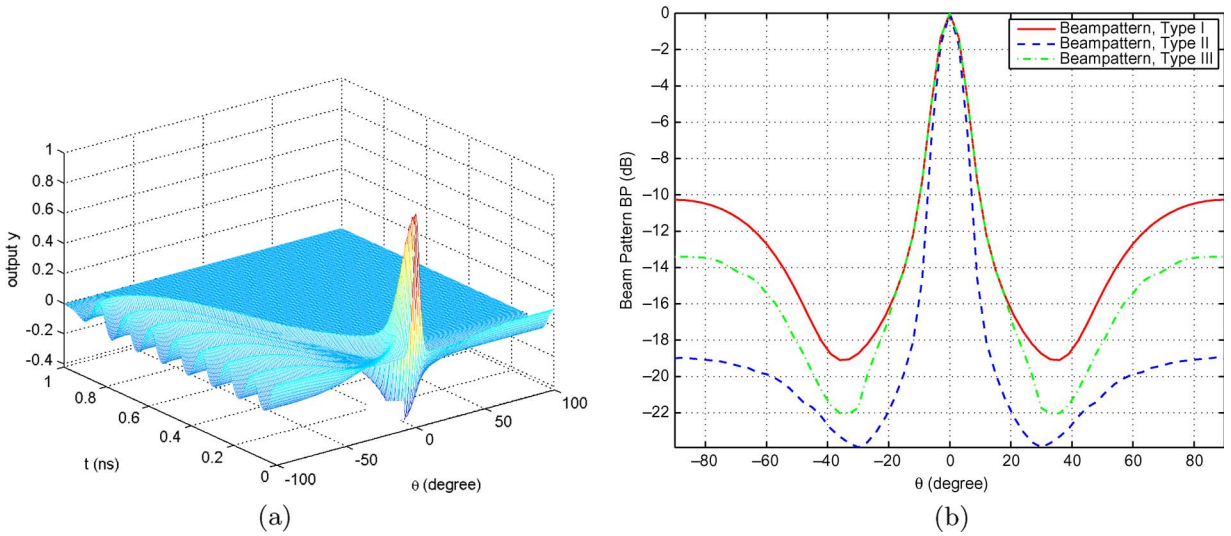

Fig. 18. *The space–time response and beam pattern of the beamformer using the monopulse in (29), where $N = 8$, $d = 3.63$ cm, $\Delta\tau = 0$, $\tau_p = 0.25$ ns, and $\xi = 1.5$. (a) Space–time response and (b) beam pattern.*

up in the lab of our Institute. It enables various experiments and testing of the proposed algorithms under real propagation constraints and scenarios.

A. Measurement Setup

VHDR applications are targeted at high-resolution media content transfer over short distances up to 1 m mainly in LOS indoor environments. The envisioned VHDRs for an extension of the existing WiMedia standard [36] vary between 1 to 3 Gbps, depending on the modulation scheme and quality of the channel. The intended doubling of the signal bandwidth to 1056 MHz and the adoption of 16-quadrature amplitude modulation (QAM) modulation inevitably place a higher level requirement to the receiver sensitivity. The receive SNR is typically required to be higher than 15 dB for reliable detection. While the system performance of single antenna VHDR has been reported to provide a sufficient small average BER at this SNR level, it is interesting to check the feasibility of MIMO approaches under the same system constraints. In particular, we have tried to examine the achievable spatial multiplexing gains and to experimentally measure the channel capacity and fading correlation under the specific test environments.

The test and verification of the VHDR MIMO MB-OFDM system were conducted within a typical office environment with desks, metal cabinets, wooden cupboards, computers, and different kinds of smaller scattering objects. For the purpose of the envisioned VHDR applications, measurements were performed in pure LOS environment. The equipment components (TX and RX) were placed on desks approximately 70 cm over the floor and 1 m apart. The transmit and receive antenna arrays were aligned linearly with 10 cm interantenna separation, corresponding to the largest wavelength of the transmitted signals. The temporal stationarity of the channel was ensured by the absence of mobile objects/persons, thus allowing us to assume quasi-static channel conditions during a single MB-OFDM frame.

The main components of the offline UWB-MIMO testbed are two AWGs and one digital phosphor oscilloscope (DPO). Each AWG supports two channels with up to 10 GSamples/s (GS/s) sampling rate and 3.5 GHz bandwidth or one channel with up to 20 GS/s sampling rate and 5.8 GHz analog bandwidth using interleaving, as well as 32 Msample memory size. Each channel may be used either for I/Q or direct intermediate/radio-frequency synthesis of arbitrary digital waveforms complying with the maximum available bandwidth. This allows for high flexibility of loading and storing various waveforms directly from a system-model simulator without the need of up-conversion circuits and expensive UWB RF front-ends. A set of various sequencing commands also enables the transmission of repetitive portions of the waveform through numerous program branches, jumps, and loops.

The DPO provides four channels with up to 50 GS/s sampling rate and 16 GHz frequency span. Therefore, it is currently possible to test and verify arbitrary 2×4 MIMO transmissions with an upper RF frequency of 5.8 GHz and 4×4 MIMO with an upper RF frequency of 3.5 GHz without additional up-conversion.

The setup of the UWB-MIMO testbed and a sketch of the whole system are illustrated in Fig. 19. As can be seen, each AWG in the testbed is connected to one UWB antenna. Since the proposed system employs spatial multiplexing, the signals are loaded into each AWG independently and transmitted synchronously over the interleave channels of each AWG. For most experiments, we have

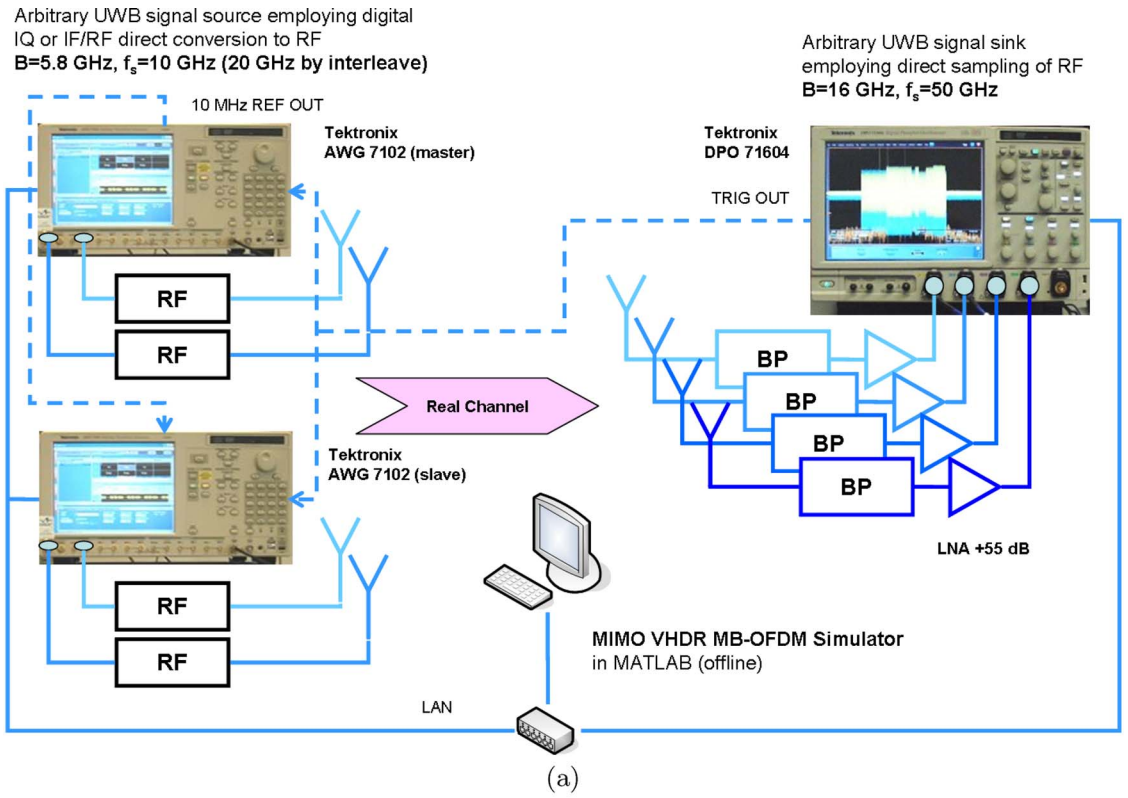

Fig. 19. ***Setup of the UWB-MIMO testbed for test and verification. (a) A sketch of system and (b) a photo of the testbed.***

used small-size omnidirectional UWB patch antennas, providing a maximum directive gain of 3 dBi in the frequency range from 3 to 4.8 GHz. In this aspect, we have limited the VHDR MIMO test to the first band group of the existing WiMedia standard [36].

On the receiver side, up to 4 UWB antennas are connected to the DPO through a bank of bandpass filters (1.5 GHz bandwidth) and +55 dB low-noise amplifiers for reliable signal acquisition under harsh SNR conditions. Note that the AWGs have been synchronized by a 10 MHz reference clock signal and separately calibrated to minimize internal RF front-end mismatches. The trigger signal of the DPO is applied to its auxiliary output, which is connected to the trigger input of the AWG. This enables synchronous MIMO transmission and reception by triggering the DPO manually with an internal command. Both AWGs and DPO are connected to the processing computer via Ethernet.

Table 2 Typical Equipment Setting for Experiments Conducted in This Paper

Parameter	Value
Channels per AWG	1 (interleaved)
AWG interleaving	on
AWG sample rate	20 GS/s
AWG sample length	20,000,000
AWG size per sample	32 bit floating point
Channels per DPO	3
DPO sample rate	25GS/s
DPO sample length	25,000,000
DPO size per sample	16 bit fixed point

B. Summary of Measured Results

An important factor in carrying out the MIMO measurements is the definition and reliable estimation of the SNR at each receive branch. For the purpose of system performance verification, there are typically two main approaches to attain different SNR levels. The first one is based on varying the power of the transmitted signal in predefined steps and repeatedly transmitting the same sequence of frames [10]. The drawback of this approach is its time-consuming and requirement of huge storage capabilities of the processing computer.

The second approach is to transmit the whole sequence of generated MB-OFDM frames with the maximum allowed equivalent isotropically radiated power, and then synthetically add colored band-limited noise to the received signal in order to vary the SNR [46]. In particular, we first estimate the actual received (maximal) SNR on each antenna branch using the PSD of the band-limited RF signal and then calculate the noise power necessary to achieve a desired SNR value. Since the received signal on each antenna is the mixture of all N_T transmitted waveforms and thermal noise, we first estimate its PSD and then subtract the average PSD of the pure noise signal between each two transmitted frames for the given frequency range. This rough estimation of the SINR has been verified using the MIMO VHDR MB-OFDM simulator under different channel models and proved reliable for the purpose of a MIMO minimum mean square error (MMSE) receiver. In the next step, we generate colored noise of predetermined average power so as to reach a desired SNR, and finally estimate its value for further use during the MMSE detection and performance measurements. In this paper, the second approach is used.

The typical equipment setting for experiments conducted in this paper is shown in Table 2. It is for the case of 2×3 UWB-MIMO offline testbed. Other cases use similar settings with some minor changes.

For every experiment, a minimum of 1000 VHDR MB-OFDM frames of 1 KB payload size are generated, sequentially transmitted and acquired by the UWB-MIMO testbed, and finally stored for further offline processing in Matlab.

Fig. 20 illustrates the power spectrum of the acquired four MIMO VHDR MB-OFDM signal frames during a 2×3 MIMO VHDR transmission. It shows a good outband suppression of the bandpass filters and gives a qualitative indication of the influence of channel fading on the received signal spectrum.

The spatial correlation coefficients between the fading paths of the estimated UWB-MIMO channel are illustrated in Fig. 21, where ρ_2^{tx} denotes the correlation coefficient between two channels from two transmit antennas to one receive antenna, and ρ_1^{rx} denotes the correlation coefficient between two channels from one transmit antenna to two receive antennas. As shown in this figure, both transmit and receive correlation coefficients are highly frequency-dependent and mostly below 0.5 with the maximum value being 0.65, which appears typically in the case where the LOS transmission is dominant. But this kind of frequency-dependence looks rather *random* with respect to the separation in frequency-domain.

The measured channel capacity is plotted in Fig. 22. As shown from both Fig. 22(a) and (b), both the ergodic capacity and outage capacity of 2×2 MIMO are approximately doubled, respectively, compared to those of the SISO case. As expected, for a fixed number of transmit antennas, each additional receive antenna provides a capacity gain that remains constant with increasing SNR.

The BER performance of the system is shown in Fig. 23. Notice that the transmission rate for the cases of two transmit antennas is doubled compared to the rate of the cases of one transmit antenna, since multiplexing is used to transmit the data symbols. It is observed that the 2×2 spatially multiplexed system provides an additional array gain of approximately 3 dB compared to the SISO. Moreover, each additional antenna at the RX is able to provide further diversity gain, as is seen when comparing 1×1 with 1×2, and 2×2 with 2×3 configurations.

VI. CONCLUDING REMARKS

In this paper, we have provided a brief overview for UWB-MIMO wireless technology covering channel capacity, space–time coding, and beamforming.

For the channel capacity, the following is shown.

i) In the MISO case, the outage probability decreases with the number of transmit antennas when the communication rate is lower than the critical transmission rate (R_c), but increases when the rate is higher than another value (R_2). R_c is determined by the fading power and the SNR of the system at the transmitter side.

ii) In the SIMO case, the communication rate supportable by the channel with a given outage

Fig. 20. ***Power spectrum of the acquired MIMO VHDR MB-OFDM frame signal.***

probability increases approximately *logarithmically* with the number of receive antennas.

iii) In the MIMO case with equal number of transmit and receive antennas, the communication rate supportable by the channel with a given outage probability increases *linearly* with the number of transmit or receive antennas.

For the space–time coding, we have shown that the 1S/2A scheme outperforms the SISO systems in BER performance according to per symbol per frame per unit energy data transmission, while the 2S/2A scheme outperforms considerably both 1S/2A scheme and SISO in BER performance when the SNR is high, but it yields (marginally or moderately) poorer BER performance than both 1S/2A scheme and SISO when the SNR is low. It is recommended to use the 1S/2A coding scheme if the number of fingers in the Rake receiver is not too large considering both the BER performance and decoding delay requirement. There exists a fundamental compromise between the available SNR and achievable spatial diversity. Basically, the spatial diversity can be exploited to gain reward only when the available SNR is sufficiently high.

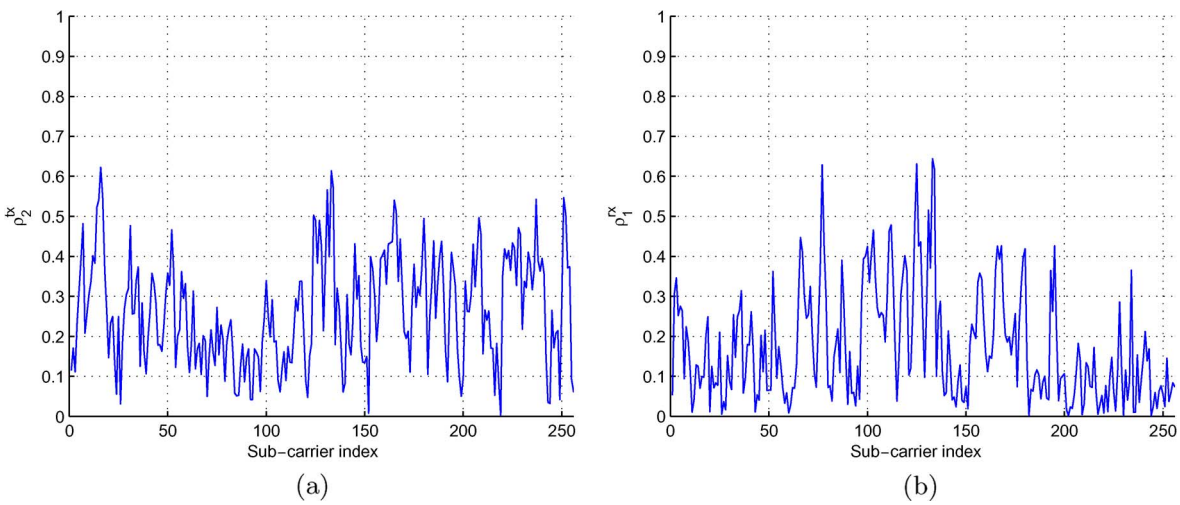

Fig. 21. ***Transmit and receive correlation coefficients.***

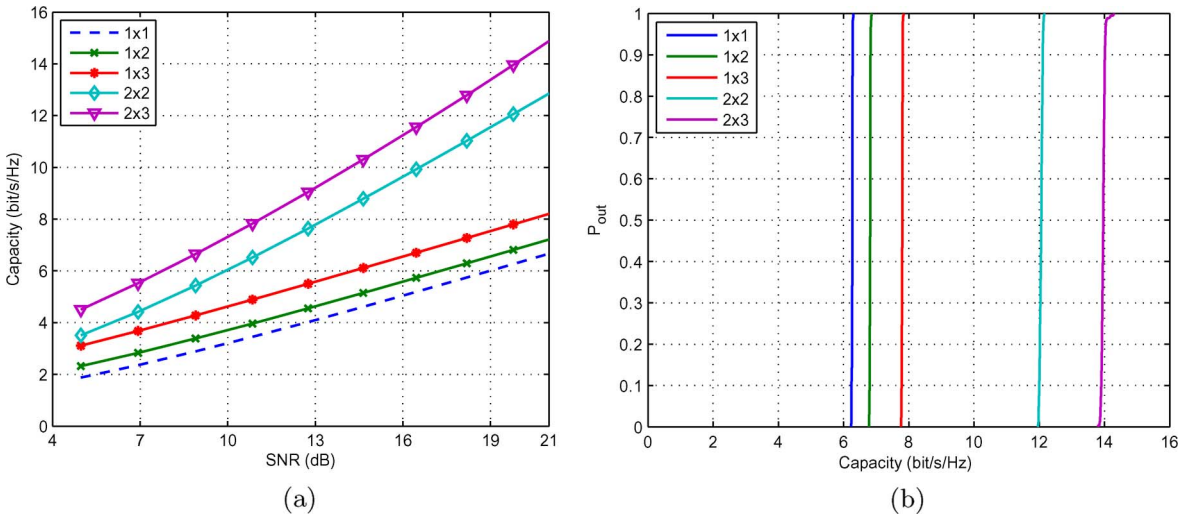

Fig. 22. ***Measured ergodic capacity and outage capacity of UWB-MIMO systems. (a) Ergodic capacity and (b) outage capacity.***

A discussion about antenna selection has been presented, and the performance comparison between the antenna selection and equal gain combiner is provided showing that the diversity gain exists in some scenarios even after the Rake processing.

For the beamforming, it is shown that the optimal beamformer is obtained if all the weighting filters $\beta_k(t)$ are identical. About the optimal beamformer, the amplitude of the side lobe is independent of the ray incidence angle if a mild condition is satisfied, which is different from the narrow-band case, and the amplitude of the main lobe is increased by a fold of the element number in the array, which is similar to the narrow-band case. Three kinds of beam patterns are defined, and the main lobe beamwidth is obtained.

It should be pointed out that the beamformer results reviewed here are obtained under rather ideal conditions, i.e., the multipath nature inherited by the UWB channel is not considered. It is reported in several studies [11], [20], [74] that in typical UWB indoor environments, the multipaths occur in a clustered way, meaning that the transmitted signal impinges the receiver from a few main directions. Based on this observation, some type of cluster beamformers can be constructed such that the main lobe width fits the cluster width so as to collect enough relevant energy, while the undesired clusters are suppressed with the array gain. In general multipath environments, challenges exist for how to properly design the corresponding beamformer.

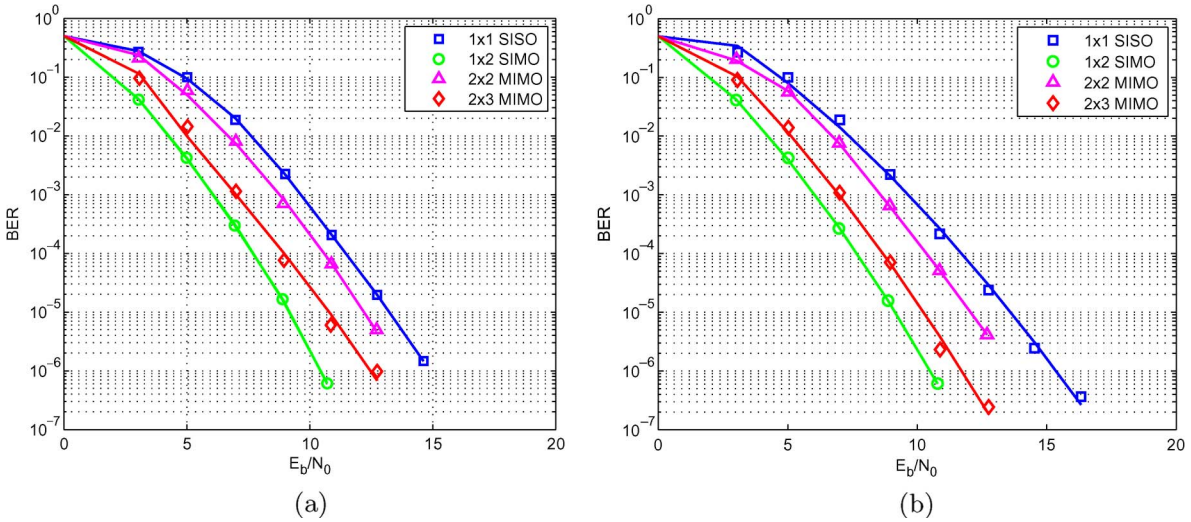

Fig. 23. ***BER performance of MIMO VHDR MB-OFDM. Coding rate $= 1/2$, 16-QAM. (a) Zero forcing and (b) MMSE.***

Experimental results based on the UWB-MIMO testbed in our lab are provided to verify some analytical results presented in this paper. ■

APPENDIX
PROOF OF PROPOSITION 1

Even though the problem is formulated in a form different from that in [60], we can use the same idea in [60] to solve the constrained maximization problem. Let us denote by $W(f)$ and $\Upsilon_k(f)$, respectively, the Fourier transforms of the signals $w(t)$ and $\beta_k(t)$. Then by the Parseval theorem, we have

$$BP_{ml} = \int_{-\infty}^{+\infty} \sum_{k_1=0}^{N-1}\sum_{k_2=0}^{N-1} |W(f)|^2 \Upsilon_{k_1}(f)\Upsilon_{k_2}^{\dagger}(f)df$$
$$BP_{sl}(\theta) = \sum_{k=0}^{N-1} \int_{-\infty}^{+\infty} |W(f)|^2 |\Upsilon_k(f)|^2 df. \quad (30)$$

For the integral in (30), applying the Schwarz inequality yields

$$\begin{aligned} BP_{ml} &= \sum_{k_1=0}^{N-1}\sum_{k_2=0}^{N-1} \int_{-\infty}^{+\infty} W(f)W^{\dagger}(f)\Upsilon_{k_1}(f)\Upsilon_{k_2}^{\dagger}(f)df \\ &\le \sum_{k_1=0}^{N-1}\sum_{k_2=0}^{N-1} \sqrt{\int_{-\infty}^{+\infty} |W(f)\Upsilon_{k_1}(f)|^2 df} \\ &\quad \cdot \sqrt{\int_{-\infty}^{+\infty} \left|W^{\dagger}(f)\Upsilon_{k_2}^{\dagger}(f)\right|^2 df} \\ &= \left[\sum_{k=0}^{N-1} \sqrt{\int_{-\infty}^{+\infty} |W(f)\Upsilon_k(f)|^2 df}\right]^2 \end{aligned} \quad (31)$$

where the equality holds if and only if

$$W(f)\Upsilon_{k_1}(f) = c_{k_1k_2} W(f)\Upsilon_{k_2}(f) \quad \text{for almost all } f \in (-\infty, +\infty) \quad (32)$$

with $c_{k_1k_2}$ being a constant depending only on the indexes k_1 and k_2. For the summation in (31), applying the Cauchy inequality yields

$$\begin{aligned} &\left[\sum_{k=0}^{N-1} \sqrt{\int_{-\infty}^{+\infty} |W(f)\Upsilon_k(f)|^2 df}\right]^2 \\ &\le \sum_{k=0}^{N-1} \int_{-\infty}^{+\infty} |W(f)\Upsilon_k(f)|^2 df \sum_{k=0}^{N-1} 1 \\ &= N \sum_{k=0}^{N-1} \int_{-\infty}^{+\infty} |W(f)\Upsilon_k(f)|^2 df \end{aligned} \quad (33)$$

where the equality holds if and only if

$$\int_{-\infty}^{+\infty} |W(f)\Upsilon_k(f)|^2 df = \varsigma \quad (34)$$

where ς is a constant and independent of k. Combining (32) and (34) gives $c_{k_1k_2} = 1$ for all k_1 and k_2. Therefore, the maximal strength for the main lobe is achieved if all the branches have the same weighting function. From (34), we can see that the constraint on the side lobes is satisfied if $\Upsilon_k(f)$ is so designed such that

$$\int_{-\infty}^{+\infty} |W(f)\Upsilon_k(f)|^2 df \le \frac{1}{N}. \quad (35)$$

This completes the proof.

Acknowledgment

The authors wish to thank their colleagues M. El-Hadidy at Leibniz University of Hannover for his completing Fig. 11 and K. Maichalernnukul, S. Sczyslo, C. Senger, B. T. Sieskul, and Z. Zhao at Leibniz University of Hannover for their helpful comments on the original version of this paper. The company IMST GmbH based in Kamp-Lintfort, Germany, is acknowledged for providing them the measured channel data. They are grateful to two anonymous reviewers for their very constructive, insightful, and detailed comments, which helped improve the quality of this paper. They are also grateful to A. F. Molisch for his initializing a proposal for them to draft this paper and his many helpful revising suggestions.

REFERENCES

[1] C. Abou-Rjeily, N. Daniele, and J.-C. Belfiore, "Differential space-time ultra-wideband communications," in *Proc. 2005 IEEE Int. Conf. Ultra-Wideband*, Zurich, Switzerland, Sep. 5–8, 2005, pp. 248–253.

[2] C. Abou-Rjeily, N. Daniele, and J.-C. Belfiore, "Diversity-multiplexing tradeoff of single-antenna and multi-antenna indoor ultra-wideband channels," in *Proc. 2006 IEEE Int. Conf. Ultra-Wideband*, Waltham, MA, Sep. 24–27, 2006, pp. 441–446.

[3] C. Abou-Rjeily, N. Daniele, and J.-C. Belfiore, "Space-time coding for multiuser ultra-wideband communications," *IEEE Trans. Commun.*, vol. 54, pp. 1960–1972, 2006.

[4] J. Adeane, W. Q. Malik, I. J. Wassell, and D. J. Edwards, "Simple correlated channel

model for ultrawideband multiple-input multiple-output systems," *IET Microw., Antennas Propag.*, vol. 1, pp. 1177–1181, 2007.

[5] B. Allen, M. Dohler, W. Q. Malik, A. K. Brown, and D. J. Edwards, Eds., *Ultra-Wideband Antennas and Propagation for Communications, Radar and Imaging*. Chichester, U.K.: Wiley, 2007.

[6] M.-G. D. Benedetto, T. Kaiser, A. F. Molisch, I. Oppermann, C. Politano, and D. Porcino, Eds., *UWB Communication Systems—A Comprehensive Overview*. New York: Hindawi, 2006.

[7] E. Biglieri, J. Proakis, and S. Shamai, "Fading channels: Information-theoretic and communications aspects," *IEEE Trans. Inf. Theory*, vol. 44, pp. 2619–2692, 1998.

[8] M. Borgmann and H. Bölcskei, "On the capacity of noncoherent wideband MIMO-OFDM systems," in *Proc. IEEE Int. Symp. Inf. Theory (ISIT)*, Adelaide, Australia, Sep. 2005, pp. 651–655.

[9] H. Bölcskei, D. Gesbert, and A. J. Paulraj, "On the capacity of OFDM-based spatial multiplexing systems," *IEEE Trans. Commun.*, vol. 50, pp. 225–234, 2002.

[10] S. Caban, C. Mehlführer, R. Langwieser, A. Scholtz, and M. Rupp, "Vienna MIMO testbed," *EUSRASIP J. Appl. Signal Process.*, pp. 1–13, 2006.

[11] C. Carbonelli and U. Mitra, "Clustered channel estimation for UWB multiple antenna systems," *IEEE Trans. Wireless Commun.*, vol. 6, pp. 970–981, 2007.

[12] D. Cassioli, M. Z. Win, and A. F. Molisch, "The ultra-wide bandwidth indoor channel: From statistical model to simulations," *IEEE J. Sel. Areas Commun.*, vol. 20, pp. 1247–1257, 2002.

[13] T.-H. Chang, Y.-J. Chang, C.-H. Peng, Y.-H. Lin, and C.-Y. Chi, "Space time MSINR-SRAKE receiver with finger assignment strategies in UWB multipath channels," in *Proc. 2005 IEEE Int. Conf. Ultra-Wideband*, Zurich, Switzerland, Sep. 5–8, 2005, pp. 242–247.

[14] Y.-L. Chao and R. A. Scholtz, "Weighted correlation receivers for ultra-wideband transmitted reference systems," in *Proc. IEEE GLOBECOM 2004*, Dallas, TX, Nov. 29–Dec. 3, 2004, pp. 66–70.

[15] S. Cherry, "Edholm's law of bandwidth," *IEEE Spectrum*, vol. 41, no. 7, pp. 58–60, 2004.

[16] C.-C. Chong, Y.-E. Kim, S. K. Yong, and S.-S. Lee, "Statistical characterization of the UWB propagation channel in indoor residential environment," *Wireless Commun. Mobile Comput.*, vol. 5, pp. 503–512, 2005.

[17] C.-C. Chong, F. Watanabe, and H. Inamura, "Potential of UWB technology for the next generation wireless communications," in *Proc. 2006 IEEE 9th Int. Symp. Spread Spectrum Tech. Applicat.*, Manaus, Amazon, Brazil, Aug. 28–31, 2006, pp. 422–429.

[18] C.-C. Chong and S. K. Yong, "A generic statistical-based UWB channel model for high-rise apartments," *IEEE Trans. Antennas Propag.*, vol. 53, pp. 2389–2399, 2005.

[19] T. M. Cover and J. A. Thomas, *Elements of Information Theory*. New York: Wiley, 1991.

[20] R. J.-M. Cramer, R. A. Scholtz, and M. Z. Win, "Evaluation of an ultra-wide-band propagation channel," *IEEE Trans. Antennas Propag.*, vol. 50, pp. 561–570, 2002.

[21] FCC, Revision of part 15 of the commission's rules regarding ultra-wideband transmission systems, FCC docket 02-48, Apr. 22, 2002.

[22] T. Kaiser and M. El-Hadidy, "A signal processing framework for MIMO UWB channels with real antennas in real environments," in *Proc. 2007 IEEE Int. Conf. Ultra-Wideband,* Singapore, Sep. 24–26, 2007.

[23] M. El-Hadidy and T. Kaiser, "An UWB channel model considering angular antenna impulse response and polarization," in *Proc. 2nd Eur. Conf. Antennas Propag.*, Edinburgh, U.K., Nov. 11–16, 2007.

[24] A. Eltaher, I. I. Ghalayini, and T. Kaiser, "Towards UWB self-positioning systems for indoor environments based on electric field polarization, signal strength and multiple antennas," in *Proc. 2nd Int. Symp. Wireless Commun. Syst.*, Sep. 5–7, 2005, pp. 389–393.

[25] A. Eltaher and T. Kaiser, "A novel approach based on UWB beamforming for indoor positioning in none-line-of-sight environments," in *Proc. RadioTeCc 2005*, Berlin, Germany, Oct. 26–27, 2005.

[26] EWC. (2005). HT PHY Specification, Enhanced Wireless Consortium Pub.ver. V1.27. [Online]. Available: http://www.enhancedwirelessconsortium.org/home/EWC_MAC_spec_V124.pdf

[27] T. Ezaki and T. Ohtsuki, "Diversity gain in ultra wideband impulse radio (UWB-IR)," in *Proc. 2003 IEEE Conf. Ultra Wideband Syst. Technol.*, Reston, Virginia, Nov. 16–19, 2003, pp. 56–60.

[28] J. R. Foerster, M. Pendergrass, and A. F. Molisch, *A channel model for ultrawideband indoor communication*. [Online]. Available: http://www.merl.com/reports/docs/TR2003-73.pdf

[29] G. J. Foschini and M. J. Gans, "On limits of wireless communications in a fading environment when using multiple antennas," *Wireless Pers. Commun.*, vol. 6, pp. 311–335, 1998.

[30] M. J. Gans, N. Amitay, Y. S. Yeh, H. Xu, T. C. Damen, R. A. Valenzuela, T. Sizer, R. Storz, D. Taylor, W. M. MacDonald, C. Tran, and A. Adamiecki, "Outdoor BLAST measurement system at 2.44 GHz: Calibration and initial results," *IEEE J. Sel. Areas Commun.*, vol. 20, pp. 570–583, 2002.

[31] M. Ghavami, "Wideband smart antenna theory using rectangular array structures," *IEEE Trans. Signal Process.*, vol. 50, pp. 2143–2151, 2002.

[32] C. Holland, "Europe approves UWB regulations," *EE Times Eur.*, May 3, 2007.

[33] B. Hu and N. C. Beaulieu, "Pulse shapes for ultrawideband communication systems," *IEEE Trans. Wireless Commun.*, vol. 4, pp. 1789–1797, 2005.

[34] M. G. M. Hussain, "Principles of space-time array processing for ultrawide-band impulse radar and radio communications," *IEEE Trans. Veh. Technol.*, vol. 51, pp. 393–403, 2002.

[35] M. G. M. Hussain, "Theory and analysis of adaptive cylindrical array antenna for ultrawideband wireless communications," *IEEE Trans. Wireless Commun.*, vol. 4, pp. 3075–3083, 2005.

[36] High Rate Ultra Wideband PHY and MAC Standard, Standard ECMA 368, ECMA Int., Dec. 2005. [Online]. Available: http://www.ecma-international.com

[37] T. Kaiser, S. Ries, and C. Senger, "UWB beamforming and DoA—Estimation," in *UWB Communication Systems—A Comprehensive Overview*, M.-G. D. Benedetto, T. Kaiser *et al.*, Eds. New York: Hindawi, 2006, pp. 330–352.

[38] T. Kaiser, C. Senger, and B. T. Sieskul, "Antenna arrays for UWB indoor localization in non-line of sight environments," in *Proc. 2006 IEEE MTT-S Int. Microwave Symp.*, San Francisco, CA, Jun. 11–16, 2006.

[39] J. Keignart, C. Abou-Rjeily, C. Delaveaud, and N. Daniele, "UWB SIMO channel measurements and simulations," *IEEE Trans. Microwave Theory Tech.*, vol. 54, pp. 1812–1819, 2006.

[40] H. Liu, R. C. Qiu, and Z. Tian, "Error performance of pulse-based ultra-wideband MIMO systems over indoor wireless channels," *IEEE Trans. Wireless Commun.*, vol. 4, pp. 2939–2944, 2005.

[41] W. Q. Malik, "MIMO capacity convergence in frequency-selective channels," *IEEE Trans. Commun.*, to be published.

[42] W. Q. Malik, "Spatial correlation in ultrawideband channels," *IEEE Trans. Wireless Commun.*, vol. 7, pp. 604–610, 2008.

[43] W. Q. Malik, B. Allen, and D. J. Edwards, "A simple adaptive beamformer for ultrawideband wireless systems," in *Proc. 2006 IEEE Int. Conf. Ultra-Wideband*, Waltham, MA, Sep. 24–27, 2006, pp. 453–457.

[44] W. Q. Malik and D. J. Edwards, "Measured MIMO capacity and diversity gain with spatial and polar arrays in ultrawideband channels," *IEEE Trans. Commun.*, vol. 55, pp. 2361–2370, 2007.

[45] W. Q. Malik and D. J. Edwards, "UWB impulse radio with triple-polarization SIMO," in *Proc. IEEE GLOBECOM'07*, Nov. 26–30, 2007, pp. 4124–4128.

[46] C. Mehlführer, S. Geirhofer, S. Caban, and M. Rupp, "A flexible MIMO testbed with remote access," in *Proc. 13th Eur. Signal Process. Conf. (EUSIPCO'05)*, Antalya, Turkey, Sep. 2005.

[47] A. F. Molisch, "MIMO systems with antenna selection: An overview," in *Proc. IEEE Radio Wireless Conf. (RAWCON)*, Aug. 2003, pp. 167–170.

[48] A. F. Molisch, "Ultrawideband propagation channels—Theory, measurement, and modeling," *IEEE Trans. Veh. Technol.*, vol. 54, no. 5, pp. 1528–1545, 2005.

[49] A. F. Molisch, M. Steinbauer, M. Toeltsch, E. Bonek, and R. S. Thomä, "Capacity of MIMO systems based on measured wireless channels," *IEEE J. Sel. Areas Commun.*, vol. 20, pp. 561–569, 2002.

[50] A. F. Molisch and M. Z. Win, "MIMO systems with antenna selection," *IEEE Micro*, vol. 5, no. 1, pp. 46–56, 2004.

[51] A. F. Molisch, M. Z. Win, and J. H. Winters, "Capacity of MIMO systems with antenna selection," in *Proc. IEEE Int. Conf. Commun.*, Helsinki, Finland, Jun. 2001, pp. 570–574.

[52] M. Médard and R. G. Gallager, "Bandwidth scaling for fading multipath channels," *IEEE Trans. Inf. Theory*, vol. 48, pp. 840–853, 2002.

[53] M. Neinhüs, M. El-Hadity, S. Held, T. Kaiser, and K. Solbach, "An ultra-wideband linear array beamforming concept considering antenna and channel effects," in *Proc. 1st Eur. Conf. Antennas Propag.*, Nice, France, Nov. 6–10, 2006.

[54] M. Neinhüs, S. Held, and K. Solbach, "FIR-filter based equalization of ultra wideband mutual coupling on linear antenna arrays," in *Proc. 2nd Int. ITG Conf. Antennas*, Munich, Germany, Mar. 28–30, 2007.

[55] T. Ohtsuki, "Space-time trellis coding for UWB-IR," in *Proc. IEEE Veh. Technol. Conf.*, Milan, Italy, May 2004, pp. 1054–1058.

[56] I. Opperman, M. Hamalainen, and J. Iinatti, *UWB Theory and Applications*. New York: Wiley, 2004.

[57] A. Paulraj, D. Gore, and R. Nabar, *Introduction to Space-Time Wireless Communications*. Cambridge, U.K.: Cambridge Univ. Press, 2003.

[58] A. J. Paulraj, D. A. Gore, R. U. Nabar, and H. Bölcskei, "An overview of MIMO communications—A key to gigabit wireless," *Proc. IEEE*, vol. 92, pp. 198–218, 2004.

[59] S. Ray, M. Medard, and L. Zheng, "On MIMO capacity in the ultra-wideband regime," in *Proc. 38th Asilomar Conf. Signals, Syst. Comput.*, Nov. 7–10, 2004, pp. 1516–1520.

[60] S. Ries and T. Kaiser, "Ultra wideband impulse beamfoming: It is a different world," *Signal Process.*, vol. 86, pp. 2198–2207, 2006.

[61] S. Sanayei and A. Nosratinia, "Antenna selection in MIMO systems," *IEEE Commun. Mag.*, vol. 42, no. 10, pp. 68–73, 2004.

[62] H. Schantz, *The Art and Science of Ultra-Wideband Antennas*. Norwood, MA: Artech House, 2005.

[63] R. A. Scholtz, D. M. Pozar, and W. Namgoong, "Ultra wideband radio," *EURASIP J. Appl. Signal Process.*, vol. 2005, pp. 252–272, 2005.

[64] W. P. Siriwongpairat, M. Olfat, and K. J. R. Liu, "Performance analysis and comparison of time-hopping and direct-sequence UWB-MIMO systems," *EURASIP J. Appl. Signal Process.*, vol. 2005, pp. 328–345, 2005.

[65] W. P. Siriwongpairat, W. Su, M. Olfat, and K. J. R. Liu, "Multiband-OFDM MIMO coding framework for UWB communication systems," *IEEE Trans. Signal Process.*, vol. 54, pp. 214–224, 2006.

[66] K. Solbach, O. Mohamed, and M. Neinhüs, "Microwave analogue FIR-filter," in *Proc. German Microw. Conf. (GeMiC) 2005*, Ulm, Germany, Apr. 5–7, 2005.

[67] W. Sörgel, C. Sturm, and W. Wiesbeck, "Impulse responses of linear UWB antenna arrays and the application to beam steering," in *Proc. 2005 IEEE Int. Conf. Ultra-Wideband*, Zurich, Switzerland, Sep. 5–8, 2005, pp. 275–280.

[68] S. S. Tan, B. Kannan, and A. Nallanathan, "Multiple access capacity of UWB M-ary impulse radio systems with antenna array," *IEEE Trans. Wireless Commun.*, vol. 5, pp. 61–66, 2006.

[69] S. S. Tan, B. Kannan, and A. Nallanathan, "Performance of UWB multiple-access impulse radio systems with antenna array in dense multipath environments," *IEEE Trans. Commun.*, vol. 54, pp. 966–970, 2006.

[70] J. D. Taylor, *Introduction to Ultra-Wideband Radar Systems*. Boca Raton, FL: CRC Press, 1995.

[71] E. Telatar, "Capacity of multi-antenna Gaussian channels," *Eur. Trans. Telecommun.*, vol. 10, pp. 585–596, 1999.

[72] I. E. Telatar and D. N. C. Tse, "Capacity and mutual information of wideband multipath fading channels," *IEEE Trans. Inf. Theory*, vol. 46, pp. 1384–1400, 2000.

[73] V. P. Tran and A. Sibille, "Spatial multiplexing in UWB MIMO communications," *Electron. Lett.*, vol. 42, no. 16, 2006.

[74] H. Tsuchiya, K. Haneda, and J.-I. Takada, "Investigation of ultra-wideband propagation channel based on a cluster scheme," *IEICE Trans. Fundam.*, vol. E89A, pp. 3095–3102, 2006.

[75] A. Tyagi and R. Bose, "A new distance notion for PPAM space-time trellis codes for UWB MIMO communications," *IEEE Trans. Commun.*, vol. 55, pp. 1279–1282, 2007.

[76] L.-C. Wang, W.-C. Liu, and K.-J. Shieh, "On the performance of using multiple transmit and receive antennas in pulse-based ultrawideband systems," *IEEE Trans. Wireless Commun.*, vol. 4, pp. 2738–2750, 2005.

[77] M. Weisenhorn and W. Hirt, "Performance of binary antipodal signaling over the indoor UWB MIMO channel," in *Proc. IEEE Int. Conf. Commun.*, Anchorage, AK, May 11–15, 2003, pp. 2872–2878.

[78] M. Z. Win, G. Chrisikos, and N. R. Sollenberger, "Performance of Rake reception in dense multipath channels: Implications of spreading bandwidth and selection diversity order," *IEEE J. Sel. Areas Commun.*, vol. 18, pp. 1516–1525, 2000.

[79] M. Z. Win and R. A. Scholtz, "Impulse radio: How it works," *IEEE Commun. Lett.*, vol. 2, no. 2, pp. 36–38, 1998.

[80] J. Winters, "On the capacity of radio communication systems with diversity in a Rayleigh fading environment," *IEEE J. Sel. Areas Commun.*, vol. SAC-5, pp. 871–878, 1987.

[81] L. Yang and G. B. Giannakis, "Multistage block-spreading for impulse radio multiple access through ISI channels," *IEEE J. Sel. Areas Commun.*, vol. 20, pp. 1767–1777, 2002.

[82] L. Yang and G. B. Giannakis, "Analog space-time coding for multiantenna ultra-wideband transmissions," *IEEE Trans. Commun.*, vol. 52, pp. 507–517, 2004.

[83] F. Zheng and T. Kaiser, "On the evaluation of channel capacity of multi-antenna UWB indoor wireless systems," in *Proc. 2004 IEEE Int. Symp. Spread Spectrum Tech. Applicat.*, Sydney, Australia, Aug. 30–Sep. 2, 2004, pp. 525–529.

[84] F. Zheng and T. Kaiser, "Channel capacity of MIMO UWB indoor wireless systems," in *UWB Communication Systems—A Comprehensive Overview*, M.-G. D. Benedetto, T. Kaiser *et al.*, Eds. New York: Hindawi, 2006, pp. 376–409.

[85] F. Zheng and T. Kaiser. (2006). "On the channel capacity of multi-antenna systems with Nakagami fading," *EURASIP J. Appl. Signal Process.* [Online]. Available: http://hindawi.com/GetArticle.aspx?doi=10.1155/ASP/2006/39436

[86] F. Zheng and T. Kaiser, "On the evaluation of channel capacity of UWB indoor wireless systems," *IEEE Trans. Signal Process.*, vol. 56, pp. 6106–6113, 2008.

ABOUT THE AUTHORS

Thomas Kaiser (Senior Member, IEEE) received the diploma degree from Ruhr-University Bochum, Germany, in 1991 and the Ph.D. (with distinction) and Habiliation degrees from Gerhard-Mercator-University, Duisburg, Germany, in 1995 and 2000, respectively, all in electrical engineering.

From 1995 to 1996, he was on research leave at the University of Southern California, Los Angeles, supported by the German Academic Exchange Service. From April 2000 to March 2001, he was Head of the Department of Communication Systems, Gerhard-Mercator-University. From April 2001 to March 2002, he was Head of the Department of Wireless Chips and Systems, Fraunhofer Institute of Microelectronic Circuits and Systems, Germany. From April 2002 to July 2006, he was Coleader of the Smart Antenna Research Team, University of Duisburg-Essen. In summer 2005, he joined the Smart Antenna Research Group, Stanford University; and in Winter 2007 Princeton's Electrical Engineering Department as a Visiting Professor. Currently, he chairs the Communication Systems Group, Leibniz University of Hannover, Germany. He is Founder and CEO of mimoOn GmbH. He has published more than 100 papers in international journals and at conferences. He was Guest Editor of several special issues and is coeditor of four books on multiantenna and ultra-wide-band systems. He serves on the Editorial Board of the *EURASIP Journal of Applied Signal Processing*. He is involved in several national and international projects, has chaired and cochaired a number of special sessions on multi-antenna implementation issues, and is a Technical Program Committee member of several conferences. His current research interest focuses on applied signal processing with emphasis on multiantenna systems, especially its applicability to ultra-wide-band systems and on implementation issues.

Dr. Kaiser was Founding Editor-in-Chief of the IEEE Signal Processing Society e-letter and is Member-At-Large of the Board of Governors of the same society. He was General Chair of the IEEE International Conference on Ultra Wideband 2008 and is General Chair of the International Conference on Cognitive Radio Oriented Wireless Networks and Communications 2009.

Feng Zheng (Senior Member, IEEE) received the B.Sc. and M.Sc. degrees in electrical engineering from Xidian University, Xi'an, China, in 1984 and 1987, respectively, and the Ph.D. degree in automatic control from Beijing University of Aeronautics and Astronautics, Beijing, China, in 1993.

He held an Alexander-von-Humboldt Research Fellowship at the University of Duisburg, Germany, and research positions with Tsinghua University, National University of Singapore, and the University of Limerick. From 1995 to 1998, he was with the Center for Space Science and Applied Research, Chinese Academy of Sciences, as an Associate Professor. Since July 2007, he has been with the Institute of Communications Technology, Leibniz University of Hannover, Germany, as a Wissenschaftlicher Beirat. His research interests are in the areas of UWB-MIMO wireless communications, signal processing, and systems and control theory.

Dr. Zheng is a corecipient of several awards, including the National Natural Science Award in 1999 from the Chinese government, the Science and Technology Achievement Award in 1997 from the State Education Commission of China, and the SICE Best Paper Award in 1994 from the Society of Instrument and Control Engineering of Japan at the 33rd SICE Annual Conference, Tokyo.

Emil Dimitrov received the M.Sc. degree in computer science and communications engineering from the University of Duiburg-Essen, Germany, in 2006. He is currently pursuing the Ph.D. degree in the area of UWB and MIMO systems at the Institute of Communications Technology, Leibniz Universität Hannover, Germany.

He has been involved in the IP6 EU Integrated Project PULSERS Phase II WP2a, where he has contributed to developing VHDR MIMO MB-OFDM system approaches. His main research interests include MIMO-, UWB-, and OFDM-based systems, transceiver architecture design, and time/frequency signal analysis.